

RESPONSE OF CARBON AND TUNGSTEN SURFACE TO DEUTERIUM AND TRITIUM PLASMAS

A Dissertation

**Submitted to the Dean Office, Institute of Science & Technology,
Tribhuvan University, Kirtipur in the Partial Fulfilment for the
requirement of Master's Degree of Science in Physics**



By

Sundar Prasad Paudel

Symbol no: 365/071

March, 2021

RECOMMENDATIONS



It is certified that Mr. Sundar Prasad Paudel has carried out the dissertation work entitled **RESPONSE OF CARBON AND TUNGSTEN SURFACE TO DEUTERIUM AND TRITIUM PLASMAS** under our supervision.

We recommend the dissertation in the partial fulfilment for the requirement for the degree of Master of Science in Physics.

Mr. Roshan Chalise
Supervisor
Department of Physics
Amrit Campus, Lainchaur
Kathmandu, Nepal

Date: 08-04-2021

Prof. Raju Khanal
Supervisor
Central Department of Physics
Tribhuvan University, Kirtipur
Kathmandu, Nepal

Date: 08-04-2021

ACKNOWLEDGEMENT

I would like to express my sincere and humble gratitude to my supervisors Prof. Raju Khanal and Mr. Roshan Chalise for their intelligent supervision, inspiring support, motivation and cooperation throughout the whole study. I had to come across the most significant academic challenge during the writing of this dissertation. It could not have been completed without the proper guidance and encouragement of my supervisors.

I would like to express my gratitude to Dr. Leela Pradhan Joshi, Head of Department, Mr. Pitambar Shrestha, coordinator MSc. Physics and Dr. Rajendra Parajuli for their valuable questions and suggestions throughout the completion of this work.

In addition, I am very grateful to all my honourable teachers of Amrit Science Campus and CDP for their valuable support and suggestions throughout my academic career. I would also like to thank all the teaching staffs of Amrit Science Campus for their support in times of need.

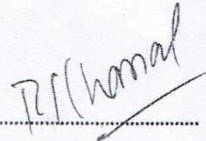
I would also like to thank my senior Mr. Yubraj Regmi all my friends especially Mr. Bishowrup Acharya, Mr. Ashok KC, Mr. Lochan Khanal, Mr. Deependra Karki, Mr. Govind Bhandari, Mr. Laxman Sedai, Mr. Sachin Paudel, Mr. Anil Thapa and all my batch-mates for their encouragement and support.

Finally, I would like to thank my Family for their support and encouragement throughout my whole academic career.

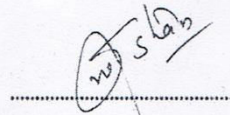
EVALUATION

We certify that we have evaluated this dissertation entitled **RESPONSE OF CARBON AND TUNGSTEN SURFACE TO DEUTERIUM AND TRITIUM PLASMAS** submitted by Mr. Sundar Prasad Paudel. In our opinion, it fulfils all the specified criteria, in the scope and quality, as a dissertation for the partial fulfilment of the requirement for the degree of Master of Science in Physics at Tribhuvan University Kirtipur, Kathmandu, Nepal.

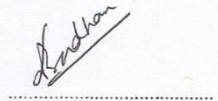
Evaluation Committee



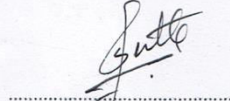
Prof. Raju Khanal
(Supervisor)
Central Department of Physics
Tribhuvan University, Kirtipur
Kathmandu, Nepal.



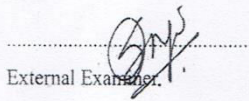
Mr. Roshan Chalise
(Supervisor)
Department of Physics
Amrit Campus, Lainchaur
Kathmandu Nepal.



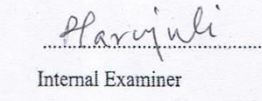
Prof. Leela Pradhan Joshi
Head, Department of Physics
Amrit Campus, Lainchaur
Tribhuvan University, Nepal



Asso. Prof. Pitamber Shrestha
MSc. Physics Program Coordinator
Amrit Campus, Lainchaur
Tribhuvan University, Nepal



External Examiner



Internal Examiner

Date: 20-04-2021

ABSTRACT

The interaction between plasma and confining material surface is crucial for better understanding of plasma-wall interactions. In this work, we have studied the interactions of carbon and tungsten surfaces in an oblique magnetic field with deuterium and tritium plasmas using Kinetic Trajectory Simulation (KTS) approach not considering the induced emissions of electrons by incident ions. The parameters including ion reflection coefficient, ion absorption coefficient, total charge density and Thomas Fermi reduced energy at various ion temperatures has been calculated. The choice of plasma facing material surface is also important to study plasma-wall interaction phenomenon. It has been observed that ion reflection coefficient decreases with the increase in ion temperature and its value is comparatively higher on tungsten wall and in tritium plasma respectively. On the other hand the ion absorption coefficient increases due to increase in projectile energy as the ion temperature increases. The total charge density increases linearly with the temperature. The Thomas Fermi reduced energy by carbon and tungsten surface are higher in deuterium plasma and also increases linearly with ion temperatures. For carbon wall the ion reflection coefficient is found to be 0.0076 at 0.5 eV and decreases to 0.0010 at 2.5 eV in deuterium plasma which slightly increases to 0.0085 and 0.0012 at the respective temperatures. Similarly for tungsten wall the ion reflection coefficient is 0.2576 and 0.1164 in deuterium plasma but is slightly higher in tritium plasma which is found to be 0.2582 and 0.1170 at 0.5 eV and 2.5 eV respectively.

Keywords: Reflection Coefficients, Ion Reflection, Ion Absorption, Plasma-Wall Interaction, Thomas Fermi Reduced Energy.

Contents

Recommendations.....	i
Acknowledgement	ii
Evaluation	iii
Abstract.....	iv
1. Introduction.....	1
1.1 Plasma	2
1.2 Plasma Criterion.....	2
1.3 Debye Shielding	3
1.4 Sheath.....	4
1.5 Presheath	5
1.6 Ion Reflection Coefficient.....	6
1.7 D-T Plasma.....	7
2. Literature Review.....	9
3. Principles and Equations of Kinetic Theory	14
3.1 Principles of Kinetic Trajectory Simulation.....	15
3.2 Basic Concepts of Kinetic Theory	15
3.3 Basic Equations Involved.....	16
3.4 Significance of Kinetic Theory	18
4. Plasma Sheath Model and Numerical Method.....	19
4.1 Description of the Model.....	20
4.2 Boundary Conditions.....	21
4.3 Presheath-Sheath Approximation.....	25
4.4 Presheath Parameters.....	25
4.5 Discretization of the Simulation Region	26
4.6 Electron Density Distribution	28

4.7 Discretizing Ion Velocity Space with a Fixed Grid	28
4.8 Ion Trajectories	29
4.9 Ion Velocity Distribution Function	33
4.10 Ion Density Distribution.....	33
4.11 Solution of Poisson's Equation.....	33
4.12 Relaxation Scheme.....	35
4.13 Iteration Scheme.....	35
4.14 Main Iteration Block	36
4.15 Convergence Check.....	36
4.16 Ion Reflection Coefficient.....	37
4.17 Numerical Parameters	39
5. Results and Discussion	40
5.1 Ion Reflection Coefficient.....	41
5.2 Ion Absorption Coefficient.....	42
5.3 Reflected Ion Density.....	44
5.4 Absorbed Ion Density.....	45
5.5 Total Charge Density	47
5.6 Thomas Fermi Reduced Energy	48
6. Conclusion and Future Works	50
6.1 Conclusion.....	51
6.2 Future Works.....	52
References.....	53
Appendix.....	56
A MATLAB files	56

Chapter 1

Introduction

1.1 Plasma

The term "plasma" was introduced by Irving Langmuir 1928 to describe the state of matter in the positive column of the glow discharge tube. Plasma is a mixture of ionized gas consisting approximately equal number of negatively charged electrons and positively charged ions. When the temperature of the gas is increased beyond a certain limit, it ionizes to the mixed population of charged particles and neutral particles called Plasma. The Characteristics of plasma are significantly different from that of the ordinary natural gases. So, Sir William Cookes identified plasma as the fourth state of matter in 1879. Plasma is the state attained by ionized gases but all ionized cases cannot be called plasma. Thus, the most suitable definition to describe plasma would be, "Plasma is quasineutral gas of charged and neutral particles which exhibit collective behaviour." Quasineutrality of plasma simply implies that the ion and electron densities are nearly equal ($n^i = n^e = n$), where n is plasma density) but not so neutral that all the intersecting electromagnetic force vanishes. The collective behaviour of plasma implies that not only local conditions but also the state of plasma far away from the point of interest also affects the motion of ions in plasma. Plasma can be created by heating a gas and subjecting it to a strong electromagnetic field applied with a laser or microwave generator. If the temperature of the gas is increased beyond a certain limit, it doesn't remain as gas; it enters into the regulated system where the thermal energy of its constituent particles overcomes the electrostatic force which binds the electrons with atomic nuclei to create plasma. Plasma is the most abundant form of ordinary matter found in the universe, most of which are found in the intergalactic region, intracluster medium in stars including the sun [1].

1.2 Plasma Criterion

Not all ionized gases can be called plasma so the mixture of interacting charged particles and neutral particles to exhibit plasma behaviour, it must satisfy following criterion.

(i) Debye length must be very short compared to the physical size of plasma;

$$\lambda_D \ll L$$

(ii) There must be a large number of particles (ions or electrons) within the Debye sphere;

$$N_D \gg 1$$

(iii) Mean time between the collisions of ions is usually long in comparison with the period of plasma oscillation; $\omega\tau \gg 1$

Where ω is the frequency of plasma oscillation and τ is the mean time between the collisions with neutral atoms [2].

1.3 Debye Shielding

The most fundamental characteristics of plasma is that, it can shield out applied electrostatic perturbations. When a test charge is inserted in the unperturbed spatially uniform and neutral plasma, the plasma gets perturbed forming a cloud of oppositely charged plasma particles, which both shields the remaining plasma from the test charge and lowers the electrostatic potential induced by the test charge to make the whole plasma to be neutral. This phenomenon is called Debye shielding. Debye shielding occurs within a very small spherical region with a radius of Debye length [3].

The mathematical expression for electron Debye length is;

$$\lambda_D = \sqrt{\frac{\epsilon_0 K_B T_e}{e^2 n}} \quad (1.1)$$

Where K_B is the Boltzmann constant, ϵ_0 is the permittivity of vacuum, T_e is the electron temperature, n is the density of electrons and e is the electronic charge. [1]

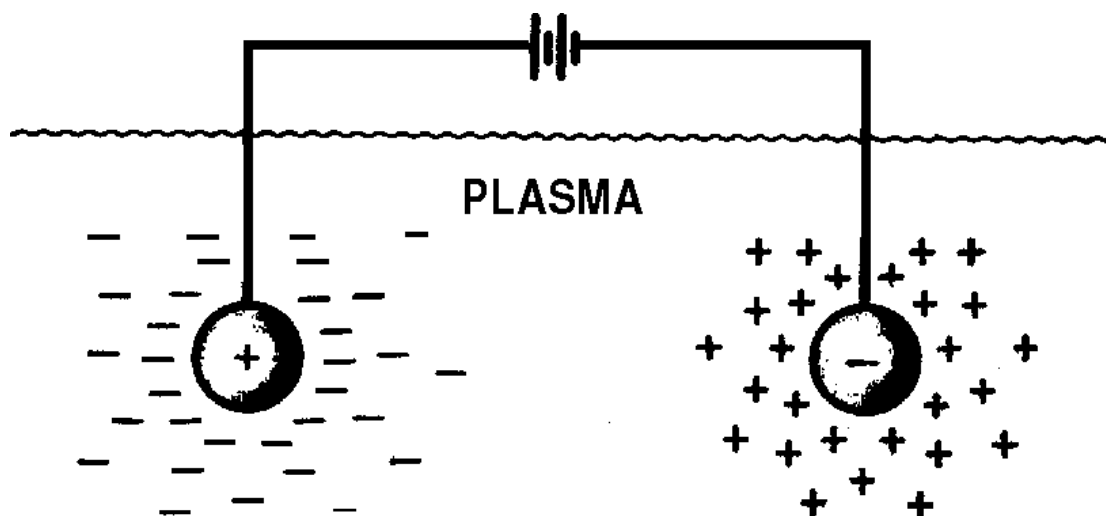


Figure1.1: Debye Shielding

1.4 Sheath

As we know electrons in plasma are much faster than ions, when plasma comes in contact with a material surface, the surface becomes negatively charged with respect to plasma potential, due to the absorption of the fast moving electrons. The negatively charged surface repels the electrons but attracts ions forming a positive space charge region called Sheath in front of material in contact with the plasma. The negative potential of the surface is effective only in the sheath region with the dimension of few Debye lengths away from the wall within the sheath region due to the shielding effect of plasma [4]. Within the sheath region, the plasma is significantly non-neutral, however becoming practically quasi-neutral at the sheath entrance or the sheath edge, the potential falls rapidly towards the wall. Due to this, the electric field is relatively strong and the motion of the plasma particles is dominated by electric forces rather than the magnetic forces. The sheath structure is responsible for the flow of the particles, and energy towards the wall may also affect the bulk plasma behaviour [5].

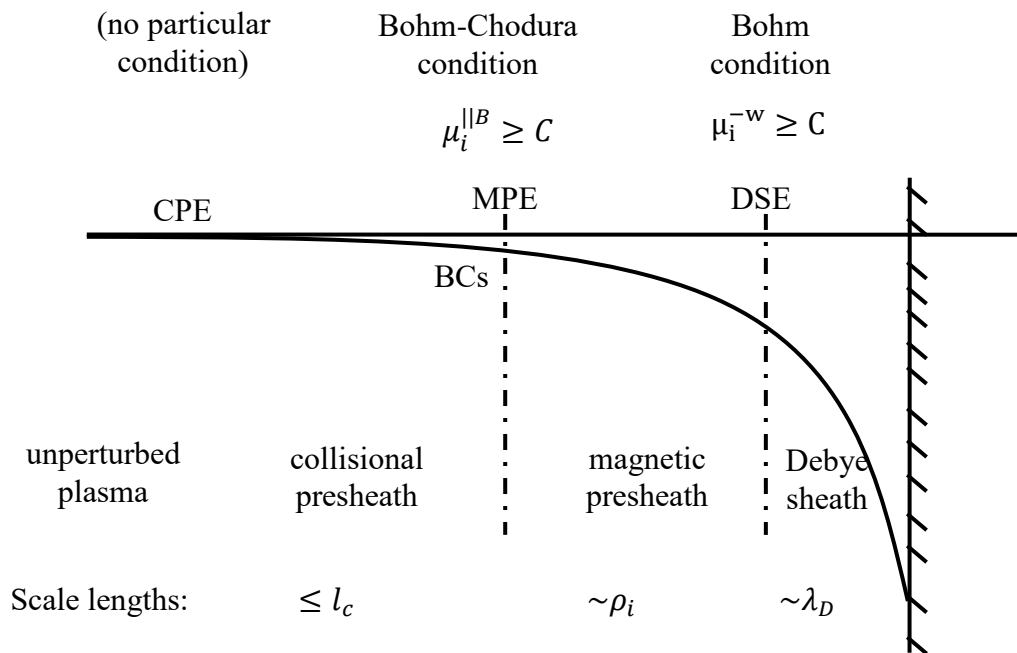


Figure: 1.2 Potential profile decreasing monotonically from $x = L$ towards $x = 0$ [6]

1.5 Presheath

Presheath region starts when the charge neutrality begins to breakdown. Since the shielding effect of the wall is not perfect; a residual electric field penetrates beyond the sheath edge deep into the bulk plasma. This forms a weak region called Presheath from where the ions are accelerated and entered into the sheath region.

For the formation of the sheath the Bohm criterion needs to be satisfied. The in-streaming ions must be accelerated up to speed equal or greater than the ion acoustic velocity at the sheath edge. This inequality can be expressed as [7];

$$\left\langle \frac{1}{v^2} \right\rangle \leq \left\langle \frac{1}{C_s^2} \right\rangle \quad (1.2)$$

Where $\langle \rangle$ denotes averaging over the ion distribution function and

$$C_s = \sqrt{\frac{K_B(\gamma^i T_i + \gamma^e T_e)}{m_i}} \quad (1.3)$$

is the ion acoustic velocity with K_B as Boltzmann Constant. Here γ^i and γ^e are the ion and electron Polytropic constants respectively and T_i and T_e are the ions and electron temperatures at the presheath side of sheath edge respectively. This condition requires that ion enters the sheath region with high velocity and the ion acceleration is also aided by an electric field penetrating the presheath region, since the thermal motion of the ions alone cannot create such an acceleration.

In the presence of non-vanishing oblique magnetic field, the presheath consists of two distinct regions. Collisional presheath adjacent to the bulk plasma, where the electron pressure gradient force accelerates electron along magnetic field lines and the magnetic Presheath adjacent to sheath, where the electric field is strong enough to deflect the ions from their motion along the magnetic field [4].

The Bohm criterion mentioned above is only for the special case when no magnetic field is applied or when magnetic field is applied perpendicular to the wall. In case of oblique magnetic field, Bohm condition is [8]

$$v_{x=\cos\theta} C_s \quad (1.4)$$

Where θ is the angle made by magnetic field along x- direction.

In magnetized plasma the ambient magnetic field B is strong enough to significantly alter particle trajectories. In particular, magnetized plasma responds differently to forces which are parallel and perpendicular to the direction of the magnetic field B .

1.6 Ion Reflection Coefficient

The ion reflection from the plasma facing materials in magnetic fusion experiments can affect the performance in fusion experiments. In tokomaks, particles confinement time is much smaller than the discharge time length due to which the average plasma ion hits a material surface and recycles back into plasma many times during a typical discharge [6].

The particle and energy reflection coefficients at plasma facing surface for hydrogen isotope plasma ions which are incident on the carbon surface are functionally dependent on the energy and angle of incidence. Thus, particle and energy reflection coefficient depends functionally on the plasma temperature and sheath potential [9].

Plasma surface interaction at the wall and diverter also introduces a controlling factor on the boundary plasma conditions through recycling and the production of impurities. In Tokomak devices, these surfaces would include the first wall, the diverter plates or limiters and any other structures close to plasma. When the ions and the neutral particles interact with the material surface, there are two possibilities [6];

- (i) It may get backscattered or reflected with some fraction of energy
- (ii) It may get permanently trapped inside the material wall.

The ion reflection is characterized by the Number Reflection Coefficient R_N , defined as the ratio of all the particles backscattered from the material surface to the number of the particles incident on the material surface; and the Energy Reflection Coefficient R_E [10].

The reflection coefficient of the light particles from the material surface varies in a systematic fashion with the projectile energy, projectile mass and the mass of the target. Here, in our case, reflection is described in terms of number reflection coefficient R_N

$$R_N = \frac{A_1 \ln(A_2 \epsilon + e)}{1 + A_3 \epsilon^{A_4} + A_5 \epsilon^{A_6}} \quad (1.5)$$

where $A_1, A_2, A_3, A_4, A_5, A_6$ depend on the mass ratio of the incoming particles to the substrate particles, e is the base of natural logarithms and ϵ is the Thomas Fermi reduced energy which can be expressed as [10];

$$\epsilon = 0.0325 \frac{\mu}{\mu+1} \frac{1}{Z_1 Z_2 \left(Z_1^{\frac{2}{3}} + Z_2^{\frac{2}{3}} \right)^{\frac{1}{2}}} E_0 \quad (1.6)$$

Where $\mu = \frac{m_2}{m_1}$, m_1 and Z_1 are the mass and charge of the incoming particles and m_2 and Z_2 are the mass and charge of the target nucleus respectively and E_0 is the projectile energy expressed in *KeV*.

Finally, ion absorption coefficient is calculated by subtracting the value of the ion reflection coefficient from the unitary value considering no possibilities of transmission.

The values of constant Hydrogen isotopes bombardment of the carbon and the tungsten atoms are presented in table [10].

Table 1: Constant values for hydrogen isotopes bombardment of carbon and tungsten.

Material	Parameter	A1	A2	A3	A4	A5	A6
Carbon	R_N	0.6192	20.01	8.922	0.6669	1.864	1.889
Tungsten	R_N	0.8250	21.41	8.606	0.6425	1.907	1.927

1.7 D-T Plasma

Fusion is a form of power generation that can create electricity by using heat from nuclear fusion devices. Fusion process needs fuel and confinement environment with enough temperature, pressure and confinement time to create plasma. Although different isotopes of light elements can be fused to achieve fusion, the deuterium and the tritium reaction has been identified as the most efficient for the fusion devices. Thus, the proposed model of the fusion reactor here generally uses Deuterium and Tritium which react more easily than Hydrogen and allow them to meet the Lawson criterion without extreme conditions. Deuterium can be distilled from all forms of water. It is widely available, with no harm and is virtually inexhaustible resource.

Tritium is a fast decaying radioelement of hydrogen which occurs only in trace quantities in nature. It can be produced during the fusion reaction through contact with the lithium. When neutrons escaping the plasma interact with the lithium, tritium can be produced. In comparison with hydrogen plasma, the lower transport in the deuterium plasma is observed in both ion and electron heat diffusivities, indicating a significant isotope effect [11].

Chapter 2
Literature Review

Irving Langmuir [12] introduced the concept of the electron temperature for measuring the temperature and the density with an electrostatic probe called Langmuir probe. He also studied the interaction of the electrons with the positive space charged ions in the sheath region to give the better understanding of the plasma sheath transition. In his works, he found that the motion of the ions means the rate at which the ions arrive at sheath is determined by the potential distribution in the plasma. Soon after Langmuir introduced plasma and developed the theory on plasma sheath, many research works have been carried out to study and understand the characteristics features of the plasma. Moreover, the choice of the plasma facing material surface and the complex plasma parameters still remain an issue for ITER [13].

Bohm [7] formulated the Bohm criterion for the formation of the sheath. Bohm criterion is an inequality stating that the in-streaming ions in the plasma be accelerated upto speed equal or greater than the ion acoustic velocity at the sheath edge. Boyd [14] suggested that Langmuir probe technique is not suitable for measuring ion densities above 1mm of Hg pressure because the probe dimension exceeds the ionic and electronic mean free paths. So he made an examination of the possibility of using a probe collecting positive ions to find ion densities. He found it possible to calculate potential distribution outside the space charge sheath, if the radius of sheath is known. He also came to a conclusion that depending on ion concentration and pressure the sheath thickness is determined around the probe and for thick sheath, thickness of the sheath must be known to get compatible solutions.

Cavaliere et al. [15] studied that, whatever may be the boundary conditions assumed for the perturbations at the plasma edge, they can never provide a coupling between the wave travelling towards the wall of finite amplitude and the one propagating into the plasma whose amplitude is divergent at the plasma boundary. Stangeby & Allen[16] demonstrated that a sufficient and necessary condition for the formation of sheath is that the plasma fields should accelerate the ions until their velocity normal to the sheath is equal to the Bohm speed, independent of the ion velocity component tangential to the sheath. Chodura [8] studied the magnetic effect on the plasma wall transition layer in an oblique magnetic field using numerical model, which simulates the motion of the plasma particles in an electric and magnetic fields for certain particle flux at plasma boundary. He also generalized the Bohm's condition for the

existence of a monotonic profile of the layer. He found the transition layer comprises of a quasineutral magnetic presheath preceding the electrostatic debye sheath. He found that the total potential drop between plasma and wall is fairly insensitive to the magnitude and the angle of magnetic field.

Riemann [17] did the kinetic analysis in the vicinity of the sheath edge that allowed him to generalize Bohms' criterion not only for arbitrary ion and electron distribution, but also for general boundary conditions at wall. He also found that, in order to fulfil Bohm criterion the ions should be pre-accelerated in quasineutral pre-sheath region dominated at least by geometric current concentration, collisional ion friction, ionization or the magnetic ion deflection. He also studied the collisional presheath in an oblique magnetic field and showed that in plane geometry, the presheath ion acceleration depends on elementary process. The main effect of a strong magnetic field is to compress the collisional presheath onto a thin layer with a characteristics extension of the ion gyro radius [18]. Ordonez & Peterjn studied the particle and energy reflection coefficients at plasma facing surface for hydrogen isotope plasma ions which are incident on the carbon surface. The expression obtained were first fit to Monte- Carlo simulation to obtain reflection coefficients which are functionally dependent on the energy and angle of incidence. The expressions thus obtained were again integrated over the distribution function for plasma ions at the sheath surface interface to obtain particle and energy reflection coefficient which depends functionally on the plasma temperature and sheath potential [9].

Luo et al. [19] studied the reflection coefficients of D-T ions in fusion plasma incident to the first wall of a fusion reactor which is necessary to understand and evaluate the energy balance, fuel recycling in the fusion reactor operation. He developed a new method based on the scaling property of ion transport for calculating the reflection coefficient of Maxwell D-T ions of fusion plasma with different temperatures. Wesson [20] investigated the effect of the temperature gradient on plasma sheath and found out that the combined effect of the dominance of fast moving electrons and the rapid decrease in the collisional frequency with velocity leads to the significant modification of the sheath and possibly also to substantial errors in the interpretation of probe signals. Chauhan et al. [21] investigated the reflection of compressive and rarefactive ion acoustic solitons propagating in the inhomogeneous plasma containing negative ions. They found out that for both compressive and rarefactive incident

solitons, amplitude goes up whereas the width decreases with increasing density ratio of negative to positive ions. It has also been found that increasing positive ion density weakens the reflection of both compressive and rarefactive solitons. Ahedo [22] investigated the influence of the magnetic field strength and the angle of incidence on the one dimensional structure of weakly collisional plasma near a charged wall and recovered the model of Chodura [7] as special case of intermediate magnetic field strength and the model of Riemann as the case of weak magnetic field strength and compared with the third case of strong magnetic field, where the space-charge sheath is partially magnetized.

Ogawa et al. [23] investigated the deuterium plasma of LHD by integrated simulation code TASK3D and 5D drift kinetic equation solver GNET. He found that more than 20% of the ion temperature increment is obtained in the deuterium plasma due to the isotope effect assuming the turbulent transport model. The tritium burn up simulation also showed that the tritium slowing down distribution and the strong magnetic configuration dependency of the tritium burn up ratio in LHD. Singha, Chutia & Sarma [24] investigated the variation of the electron temperature and the plasma density in a magnetized plasma experimentally in the presence of a grid placed at the middle of the system. It was revealed that with increasing magnetic field and negative grid biasing voltage, the sheath thickness expands. Franklin [25] investigated the significance of the Bohm criterion in an active collisional plasma sheath and concluded that the ions remain in collisional equilibrium with the electric field and there is no such thing as a collisionally modified Bohm criterion.

Crowley [26] developed the method for modelling the electrical conductivity of dense multicomponent plasma using well-known Ziman formula in hot Lorentzian plasmas as well as to systems of arbitrary electron degeneracy. Kawata & Ohya [27] developed a Monte Carlo simulation model to study the ion reflection and sputtering for plasma irradiated surface in an oblique magnetic field and found that some of the emitted particles were ionized and gyrated in the plasma immersed in an oblique magnetic field. Zhang, Shen & Yu [28] studied the effect of plasma temperature on electrostatic shock generated by circularly polarized laser pulse in overdense plasma using PIC simulation and found that the ions are much more accelerated at low but finite temperatures than when they were cold. Kaufmann & Neu [29] studied the use of tungsten as first wall material in fusion devices. They studied the physical side of

the interaction between plasma and the tungsten wall surface and the transport of tungsten in the plasma boundary and also in the core.

Khanal [30] developed a Kinetic Trajectory Simulation (KTS) model for $1D1V$, time independent, collision less bounded plasma for the modelling of various situation of interest with high accuracy. Electrons were supposed to have half Maxwellian velocity distribution function at injection so their density can be calculated analytically. While on the other hand, the exact ion trajectories are followed to calculate ion distribution function assuming arbitrary ion distribution at injection. The method is exemplarily applied to a single emitter diode and one dimensional plasma sheath. In this method, starting from the initial guess, the potential profile is iterated towards the final time independent self-consistent rate.

Chalise & Khanal [31] studied the magnetized plasma wall transition in an oblique magnetic field. He used KTS model to obtain the final self-Consistent solution to the time independent, collision less plasma for the given electron and ion density distribution at the Sheath entrance. The plasma parameters reaching the material wall is insensitive to the magnitude and orientation of the magnetic field but is highly influenced near the sheath entrance. Thus, he found that the electric field doesn't show the usual monotonic nature at the magnetic presheath region. Chalise and Khanal [32] presented the KTS model for magnetized plasma sheath and found out that the magnetic effect is prominent near the Sheath entrance and has almost no effect at the wall. They also developed a self-consistent one dimensional in space and three dimensional in velocity ($1D3V$) Kinetic Trajectory Simulation Model of magnetized plasma wall transition for the study of the various types of plasma sheaths [33].

Chapter 3

Principles and Equations of Kinetic Theory

3.1 Principles of Kinetic Trajectory Simulation

In the Kinetic Trajectory Simulation (KTS) method the velocity distribution function of particle species involved are directly calculated by solving the related kinetic equations along the respective collisionless particle trajectories. In order to obtain the distribution function at any point of the phase-space we trace the related trajectories of phase-space where the distribution function is given. Here, we assume the electron and ion velocity distribution functions at the sheath edge to be cut-off Maxwellian [30].

KTS is an iterative method for numerically calculating self-consistent, time-independent kinetic plasma states in some given bounded spatial region. The plasma states are generally characterized by [1];

- the velocity distribution function $f(\vec{x}, \vec{v}, t)$
- the electric field $\vec{E}(\vec{x})$
- the magnetic field $\vec{B}(\vec{x})$
- the given boundary conditions.

3.2 Basic Concepts of Kinetic Theory

In the general case of time-dependent, collisional kinetic theory, the species-s velocity distribution function satisfies the kinetic equation.

$$\begin{aligned} \frac{df^s}{dt} &= \left(\frac{\partial}{\partial t} + \vec{v} \cdot \frac{\partial}{\partial \vec{x}} + a^s \cdot \frac{\partial}{\partial \vec{v}} \right) f^s(\vec{x}, \vec{v}) \\ &= C^s \end{aligned} \quad (3.1)$$

with

$$\vec{a}(\vec{x}, \vec{v}, t) = \frac{q^s}{m^s} [\vec{E}(\vec{x}, t) + \vec{v} \times \vec{B}(\vec{x}, t)] \quad (3.2)$$

Here, the locally averaged electric and magnetic fields are $\vec{E}(\vec{x}, t)$ and $\vec{B}(\vec{x}, t)$, the macroscopic acceleration of the species-s particles is $\vec{a}^s(\vec{x}, \vec{v}, t)$ and C^s is the species-s collision term. The time derivative

$$\frac{d}{dt} = \left(\frac{\partial}{\partial t} + \vec{v} \cdot \frac{\partial}{\partial \vec{x}} + a^s \cdot \frac{\partial}{\partial \vec{v}} \right) \quad (3.3)$$

is the ‘‘Lagrangian’’ or total time derivative along the species- s trajectory. For collisionless cases the kinetic equation Eq. (3.1) takes the well-known form of ‘‘Vlasov equation’’ [1]

$$\left(\frac{\partial}{\partial t} + \vec{v} \cdot \frac{\partial}{\partial \vec{x}} + a^{\vec{s}} \cdot \frac{\partial}{\partial \vec{v}}\right) f^s = 0 \quad (3.4)$$

i.e.

$$\begin{aligned} \frac{d_s f^s}{dt} &= 0 \\ f^s &= \text{constant} \end{aligned} \quad (3.5)$$

This means that the velocity distribution function is constant for an observer moving along a collisionless trajectory. Hence, the distribution function at every point along the trajectory can be obtained if its value at one point is known. Here we assume the boundary distribution function is given.

3.3 Basic Equations Involved

The following basic equations correspond to one-dimensional, time-independent, collisionless, electrostatic problems.

(a) For electrons ($q = -e$), the velocity distribution functions satisfy the time-independent Vlasov equation in differential forms as

$$\frac{d f^e}{dt} = \left[\vec{v} \cdot \frac{\partial}{\partial \vec{x}} - \frac{e}{m^e} \left(\vec{E}(\vec{x}) + (\vec{v} \times \vec{B}(\vec{x})) \right) \cdot \frac{\partial}{\partial \vec{v}} \right] f^e(\vec{x}, \vec{v}) \quad (3.6)$$

The electron equations of motion are:

$$\frac{d \vec{x}^e}{dt} = \vec{v}_x^e \quad (3.7)$$

and velocity component

$$\frac{d \vec{v}_x^e}{dt} = \vec{a}_x^e \quad (3.8)$$

$$\frac{d \vec{v}_y^e}{dt} = \vec{a}_y^e \quad (3.9)$$

$$\frac{d \vec{v}_z^e}{dt} = \vec{a}_z^e \quad (3.10)$$

with the macroscopic acceleration component defined by,

$$\vec{a}_x^e = \frac{e}{m^e} \left[\vec{E}(\vec{x}) + (\vec{v} \times \vec{B}(\vec{x})) \right]_x \quad (3.11)$$

$$\vec{a}_y^e = \frac{e}{m^e} [\vec{E}(\vec{x}) + (\vec{v} \times \vec{B}(\vec{x}))_y] \quad (3.12)$$

$$\vec{a}_z^e = \frac{e}{m^e} [\vec{E}(\vec{x}) + (\vec{v} \times \vec{B}(\vec{x}))_z] \quad (3.13)$$

(b) Similarly, for the singly charged ions, ($q = +e$), the velocity distribution functions satisfy the time independent Vlasov equations in differential form as

$$\frac{df^i}{dt} = \left[\vec{v} \frac{\partial}{\partial \vec{x}} - \frac{e}{m^i} (\vec{E}(\vec{x}) + \vec{v} \times \vec{B}(\vec{x})) \frac{\partial}{\partial \vec{v}} \right] f^i(\vec{x}, \vec{v}) \quad (3.14)$$

The ion equations of motion are:

$$\frac{d\vec{x}^i}{dt} = \vec{v}_x^i \quad (3.15)$$

and velocity component

$$\frac{d\vec{v}_x^i}{dt} = \vec{a}_x^i \quad (3.16)$$

$$\frac{d\vec{v}_y^i}{dt} = \vec{a}_y^i \quad (3.17)$$

$$\frac{d\vec{v}_z^i}{dt} = \vec{a}_z^i \quad (3.18)$$

with the acceleration component is given by,

$$\vec{a}_x^i = \frac{e}{m^i} [\vec{E}(\vec{x}) + (\vec{v} \times \vec{B}(\vec{x}))_x] \quad (3.19)$$

$$\vec{a}_y^i = \frac{e}{m^i} [\vec{E}(\vec{x}) + (\vec{v} \times \vec{B}(\vec{x}))_y] \quad (3.20)$$

$$\vec{a}_z^i = \frac{e}{m^i} [\vec{E}(\vec{x}) + (\vec{v} \times \vec{B}(\vec{x}))_z] \quad (3.21)$$

(c) The electrostatic potential $\phi(x)$ is to be found from Poisson's equation

$$\frac{d^2\phi(x)}{dx^2} = \frac{\rho(x)}{\epsilon_0} \quad (3.22)$$

The space charge density is defined as,

$$\rho(x) = \sum_s q^s n^s(x_j) \quad (3.23)$$

With the electron and ion densities given as

$$n^s(x) = \int_{-\infty}^{\infty} dv f^s(x, v), s = (e, i) \quad (3.24)$$

These equations are solved iteratively for given field and particle boundary conditions.

(d) The ion reflection coefficient is defined as [10],

$$R_N = \frac{A_1 \ln(A_2 \epsilon + e)}{1 + A_3 \epsilon^{A_4} + A_5 \epsilon^{A_6}} \quad (3.25)$$

and Thomas Fermi reduced energy is given by [10],

$$\epsilon = 0.0325 \frac{\mu}{\mu+1} \frac{1}{Z_1 Z_2 \left(Z_1^{\frac{2}{3}} + Z_2^{\frac{2}{3}} \right)^{\frac{1}{2}}} E_0 \quad (3.26)$$

(e) The ion absorption coefficient is given by,

$$R_A = 1 - R_N \quad (3.27)$$

3.4 Significance of Kinetic Theory

It is insufficient to describe plasma using fluid model and requires the consideration of velocity distribution which leads us to the kinetic theory. The kinetic theory of plasma not only describes but also predicts the overall condition of plasma from the macroscopic interactions and the motion of its constituent particles. It also deals with the relationship between velocity and forces and the study of particles in velocity space. It provides an essential basis in the introduction to plasma physics and subsequently advanced kinetic theory. The knowledge of the plasma parameters helps us to understand the dynamics of plasma. The most important of these parameters include plasma temperature, plasma density, Debye shielding and Debye length. The conditions in the plasma strongly depend on the distribution of the charged particles over a velocity space. Thus kinetic theory is more significant for the better understanding of the plasma behaviours [34].

Chapter 4

Plasma Sheath Model and Numerical Method

The Kinetic trajectory Simulation Method [30, 32] has been adopted and modified according to our considerations.

4.1 Description of the Model

We first consider the 1d3v model [32] of collisionless bounded plasma as shown in Figure 4.1. In this work, we restrict ourselves to the energy of projectile particles lie between 10 eV to 100 keV and considered an oblique magnetic field. The electron emission from the wall induced by incoming ion is neglected for both deuterium and tritium plasmas.

Here the right hand boundary is the region from where our sheath region starts which is also called the sheath entrance which generally separates out the collisionless and non-neutral sheath region from the bulk plasma and in the left hand region there is partially absorbing material wall of carbon and tungsten.

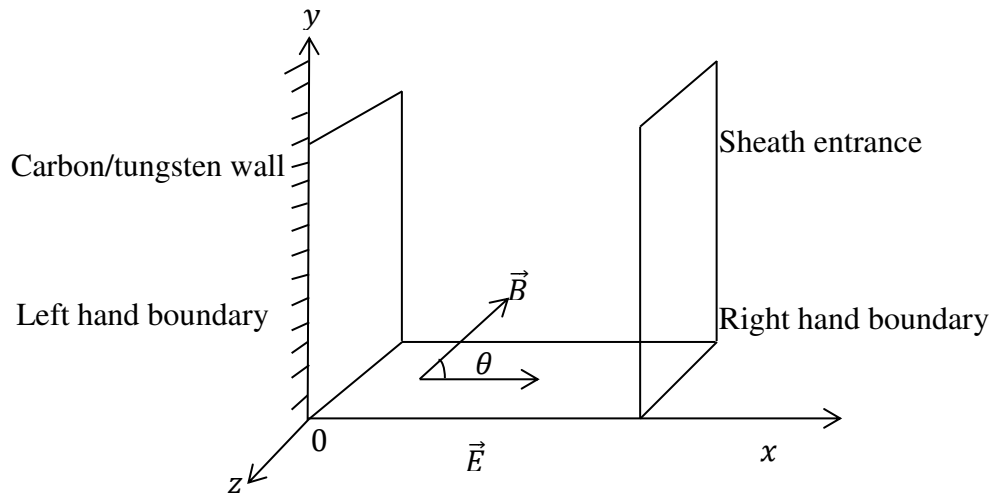


Figure 4.1: Plasma sheath model [32].

We are assuming that the angle between an oblique magnetic field along with the x -axis and denoted by θ . Here electric field is along x -axis. For simplicity, consider the plasma parameter vary only along x -direction. At $\theta = 0$ magnetic field is perpendicular to the wall or parallel to the electric field. And at $\theta = \frac{\pi}{2}$, magnetic field is parallel to the wall or perpendicular to the electric field. The resultant magnetic field is

$$B = B_0[\cos\theta\hat{x} + \sin\theta\hat{y}] \quad (4.1)$$

Hence, in this case the plasma sheath is collisionless time independent and electrostatic.

4.2 Boundary Conditions

To solve the set of equations compiled in Sec.(2.3), we need to know the boundary conditions for the velocity distribution functions (particle boundary conditions) and the potential (field boundary conditions) and the potential (field boundary conditions) at the two boundaries of the simulation region. The boundary potentials $\phi(x = 0)$ and $\phi(x = L)$, the boundary injection distribution function $f^s(L, v)$ and the distribution function at the wall $f^s(0, v)$ are considered to be given. Hence, they must be specified before the iteration is started and are kept constant throughout the entire simulation.

(a) Particle Boundary Conditions

Here, we consider that the plasma particle enters the simulation region for the right-hand boundary with cut-off Maxwellian velocity distributions functions the left hand boundary absorb some fraction of particles that depends on the energy of incident particles. Due to this, the distribution function satisfies the following boundary conditions.

$$f^s(x = 0, v \leq 0) = 0 \quad s = (e, i) \quad (4.2)$$

at the left-hand boundary.

$$f^e(x = L, v \leq 0) = A^e \exp \left[- \left(\frac{m^e (v_x^2 + v_y^2 + v_z^2)}{2kT_f^e} \right) \right] \quad (4.3)$$

$$f^e(x = L, v \leq 0) = A^e \exp \left[- \left(\frac{v_x^2 + v_y^2 + v_z^2}{(v_{tf}^e)^2} \right) \right]$$

and

$$f^i(x = L, v \leq 0) = A^i \exp \left[- \frac{m^i [(v_x^i - v_{mL}^i)^2 + (v_y^i)^2 + (v_z^i)^2]}{2kT_f^i} \right] \Theta(v_{cL}^i -) v_x \quad (4.4)$$

Where T_f^e and T_f^i and are the electron and ion thermal temperature respectively, v_{tf}^s is the thermal velocity of species particle given by,

$$v_{tf}^s = \sqrt{\frac{2kT_f^s}{m^s}} \quad (4.5)$$

v_{mL}^i is the ion "Maxwellian-maximum" velocity at $x = L$. Also v_{cL}^i (with $v_{cL}^i < 0$) is the ion cut-off velocity at $x = L$. Where $\Theta(x)$ is the Heaviside function whose value is 1 if $x \geq 0$ otherwise zero.

As we are considering the electrons enter at injection plane with half Maxwellian and out potential profile is decreasing monotonically towards the left-hand boundary. So, the electron velocity distribution function is given by,

$$f^e(x, v) = A^e \exp \left[- \left(\frac{v_x^2 + v_y^2 + v_z^2}{(v_{tf}^e)^2} \right) + \frac{e\phi(x)}{kT_f^e} \right] \Theta(v_{cL}^e(x) - v_x) \quad (4.6)$$

where,

$$v_c^e(x) = \sqrt{\frac{2e[\phi(x) - \phi_0]}{m^e}} \quad (4.7)$$

is the electron cut-off velocity at point x .

For $x = L$, in particular we have,

$$f^e(x = L, v) = A^e \exp \left[- \left(\frac{v_x^2 + v_y^2 + v_z^2}{(v_{tf}^e)^2} \right) \right] \Theta(v_{cL}^e - v_x) \quad (4.8)$$

where,

$$v_{cL}^e = \sqrt{\frac{-2e\phi_0}{m^e}} \quad (4.9)$$

Similarly, from Eq. (4.2-4.7) and using the fact that our potential profile is monotonically decreasing towards the wall or electrode (left-hand boundary) and ions enter the sheath entrance with cut-off Maxwellian velocity distribution function, we get the total velocity distribution function at $x = L$ as

$$f^i(x = L, v) = A^i \exp \left[- \left(\frac{(v_x^i - v_{mL}^i)^2 + (v_y^i)^2 + (v_z^i)^2}{(v_{tf}^i)^2} \right) \right] \Theta(v_{cL}^i - v_x) \quad (4.10)$$

In the right-hand side of the Eq.(3.8) and Eq. (3.10), there are seven parameters, $A^e, T_f^e, v_{cL}^e,$

A^i, T_f^i, v_{mL}^i and v_{cL}^i which must be specified according to the physical situation considered. Now the particle density and other physical parameters at $x = L$ are given by

$$n_L^e = \int_{-\infty}^{+\infty} d^3v f^e(L, v) \quad (4.11)$$

$$n_L^i = \int_{-\infty}^{+\infty} d^3v f^i(L, v) \quad (4.12)$$

For the velocity distribution given by Eq. (4.8), we evaluate Eq. (4.11) for electron.

The electron density at $x = L$ is

$$\begin{aligned} n_L^e &= \int_{-\infty}^{\infty} d^3v f^e(L, v) \\ &= \int_{-\infty}^{\infty} dv_x \int_{-\infty}^{\infty} dv_y \int_{-\infty}^{\infty} dv_z A^e \exp \left[- \left(\frac{(v_x^2 + v_y^2 + v_z^2)}{(v_{tf}^e)^2} \right) \right] \Theta(v_{cL}^e(x) - v_x) \\ n_L^e &= A^e \int_{-\infty}^{v_{cL}^e} dv_x \exp \left[- \left(\frac{v_x}{v_{tf}^e} \right)^2 \right] \int_{-\infty}^{\infty} dv_y \exp \left[- \left(\frac{v_y}{v_{tf}^e} \right)^2 \right] \int_{-\infty}^{\infty} dv_z \exp \left[- \left(\frac{v_z}{v_{tf}^e} \right)^2 \right] \end{aligned} \quad (4.13)$$

Using

$$\left(\frac{v_x}{v_{tf}^e} \right) = \xi, \text{ we get}$$

$$\begin{aligned} n_L^e &= A^e \int_{-\infty}^{v_{cL}^e} d\xi v_{tf}^e \exp(-\xi^2) d\xi \times \sqrt{\Pi(v_{tf}^e)^2} \times \sqrt{\Pi(v_{tf}^e)^2} \\ &= A^e \Pi(v_{tf}^e)^3 \left[\frac{\sqrt{\pi}}{2} + \frac{\sqrt{\pi}}{2} \operatorname{erf} \left(\frac{v_{cL}^e}{v_{tf}^e} \right) \right] \\ &= \frac{\pi^{\frac{3}{2}} (v_{tf}^e)^3 C^e A^e}{2} \end{aligned} \quad (4.14)$$

Where,

$$\begin{aligned} C^e(T_f^e, \Phi_0) &= 1 + \operatorname{erf} \left(\frac{v_{cL}^e}{v_{tf}^e} \right) \\ &= 1 + \operatorname{erf} \sqrt{\frac{-e\Phi_0}{kT_f^e}} \end{aligned} \quad (4.15)$$

and 'erf' represents the "error function" which is defined as

$$\operatorname{erf}(x) = \frac{2}{\sqrt{\pi}} \int_0^x d\xi \exp(-\xi^2) \quad (4.16)$$

Now, from the velocity distribution function, Eq. (4.10) and Eq. (4.12), we get ion density as,

$$\begin{aligned}
n_L^i &= \int_{-\infty}^{+\infty} d^3v f^i(L, v) \\
&= \int_{-\infty}^{+\infty} d^3v A^i \exp \left[- \left(\frac{(v_x^i - v_{mL}^i)^2 + (v_y^i)^2 + (v_z^i)^2}{(v_{tf}^i)^2} \right) \right] \Theta(v_{cL}^e - v_x) \\
&= \int_{-\infty}^{\infty} dv_x \int_{-\infty}^{\infty} dv_y \int_{-\infty}^{\infty} dv_z A^i \exp \left[- \left(\frac{((v_x^i)^2 - v_{mL}^i)^2 + (v_y^i)^2 + (v_z^i)^2}{(v_{tf}^i)^2} \right) \right] \Theta(v_{cL}^i(x) - v_x)
\end{aligned}$$

$$n_L^i = A^i \int_{-\infty}^{v_{cL}^i} dv_x \exp \left[- \left(\frac{v_x^i - v_{mL}^i}{v_{tf}^i} \right)^2 \right] \int_{-\infty}^{\infty} dv_y \exp \left[- \left(\frac{v_y^i}{v_{tf}^i} \right)^2 \right] \int_{-\infty}^{\infty} dv_z \exp \left[- \left(\frac{v_z^i}{v_{tf}^i} \right)^2 \right]$$

Using

$$\left(\frac{v_x^i - v_{mL}^i}{v_{tf}^i} \right) = \xi, \text{ then limit;}$$

At $v_x = -\infty, \xi = -\infty$ and

$$\text{At } v_x = v_{cL}, \xi = \frac{v_{cL}^i - v_{mL}^i}{v_{tf}^i}$$

$$\begin{aligned}
n_L^i &= A^i \int_{-\infty}^{\frac{v_{cL}^i - v_{mL}^i}{v_{tf}^i}} d\xi v_{tf}^i \exp(-\xi^2) d\xi \times \sqrt{\Pi(v_{tf}^i)^2} \times \sqrt{\Pi(v_{tf}^i)^2} \\
&= A^i \Pi(v_{tf}^i)^3 \left[\frac{\sqrt{\pi}}{2} + \frac{\sqrt{\pi}}{2} \operatorname{erf} \left(\frac{v_{cL}^i}{v_{tf}^i} \right) \right] \tag{4.17}
\end{aligned}$$

$$= \frac{\pi^{3/2} (v_{tf}^i)^3 C^i A^i}{2} \tag{4.18}$$

where,

$$C^i = 1 + \operatorname{erf}(\Gamma_{cL}^i) \tag{4.19}$$

and

$$\Gamma_{cL}^i = \left(\frac{v_{cL}^i - v_{mL}^i}{v_{tf}^i} \right) \tag{4.20}$$

We can also define the "complementary error function" as

$$\operatorname{erfc}(x) = 1 - \operatorname{erf}(x) \tag{4.21}$$

(b) Field Boundary Conditions

The potential profile at $x = L$ is chosen as zero, whereas the one at $x = 0$ is fixed to a negative constant value, i.e.

$$\phi(x = 0) = \phi_0 = \text{const.} < 0 \quad (4.22)$$

$$\begin{aligned} \phi(x = L) &= \phi(L) \\ &= 0 \end{aligned} \quad (4.23)$$

We restrict ourselves to the potential distribution which decreases monotonically from $x = L$ to $x = 0$ such that the electric field is always negative as shown in Figure 1.2.

4.3 Presheath-Sheath Approximation

The plasma flowing towards the plasma transition region to a wall passes through two regions: the narrow region in which there is large gradient of electric field and supersonic velocity known as "sheath" and the region attached with the side of bulk plasma in which relatively weak gradient of variables and in general subsonic flow known as "presheath".

The scale lengths of the sheath and presheath are different. So, usually they are studied separately using different models and methods [6]. However, for our case to couple the different solutions at the presheath and sheath side is important. This coupling scheme satisfies the most crucial requirement of the presheath-sheath transition, i.e. quasineutrality, the sheath edge singularity condition and kinetic Bohm criterion. In the numerical method section, we show the discretization of the simulation region.

4.4 Presheath Parameters

We assume that the parameters at the presheath side of the sheath region are given or can be obtained by velocity distribution function. Let us assume the ion and electron densities,

$$n_{ps}^e = n_{ps}^i \quad (4.24)$$

and the condition of sheath formation

$$u_{ps}^i = -C_s \cos \theta \quad (4.25)$$

where, θ is the angle made by the magnetic field, and

$$C_i = \sqrt{\frac{k\gamma^i T_{ps}^i + \gamma^e T_{ps}^e}{m^i}} \quad (4.26)$$

Also, the electric current density at presheath region is defined by

$$j_{ps} = e(n_{ps}^i u_{ps}^i - n_{ps}^e u_{ps}^e) \quad (4.27)$$

and the sheath-edge plasma density,

$$n_{ps}^e = u_{ps}^i - n_{ps} \quad (4.28)$$

In summary, at the sheath edge ($x = L$) our two-fluid presheath plasma is can be characterized by the presheath parameters: n_{ps}^e , n_{ps}^i , u_{ps}^i , u_{ps}^e , T_{ps}^i , T_{ps}^e , C_s and j_{ps} , which are related by conditions Eq. (4.24) - Eq. (4.28).

Thus, for the given presheath parameters the corresponding sheath parameters can be obtained by solving these coupling equations.

4.5 Discretization of the Simulation Region

We are interested only in the region between $x = 0$ and $x = L$, which we called 'simulation region'. The entire simulation region is discretised uniformly in configuration and velocity space, as shown in fig. 4.2. Here, the position grid point in this region is denoted as x_j ($j = 1, 2, 3, \dots, n_x$, with n_x the total number of grid points) and the separation between consecutive grid points is denoted by Δx . In our discretization, $j = 1$ and $j = n_x$ correspond to the left-hand boundary ($x = 0$) and the right-hand boundary ($x = L$) respectively. In our computations we choose the region to be large enough such that the grid size is always less than the Debye length of the injected electrons. If the values of any quantity $Q(x)$ at the grid points are denoted as $Q_j = Q(x_j)$, its value at any point ' x ' between two grid points Q_j and Q_{j+1} can be approximated by means of linear interpolation in the form,

$$Q(x) = \left(\frac{x_{j+1}-x}{\Delta x}\right) Q_j + \left(\frac{x-x_j}{\Delta x}\right) Q_{j+1} \quad (4.29)$$

where $x_j \leq x \leq x_{j+1}$. Another standard approximation is the second-order interpolation between the points x_{j-1} and x_{j+1} .

$$Q_x = Q_j + a(x - x_j) + b(x - x_j)^2 \quad (4.30)$$

and at point $x = x_{j-1}$

$$Q_{j-1} = Q_j - a\Delta x + b\Delta x^2 \quad (4.31)$$

and at point $x = x_{j+1}$

$$Q_{j+1} = Q_j + a\Delta x + b\Delta x^2 \quad (4.32)$$

Form Eq. (4.31)

$$a = \left(\frac{Q_j - Q_{j-1} + b(\Delta)^2}{\Delta x} \right) \quad (4.33)$$

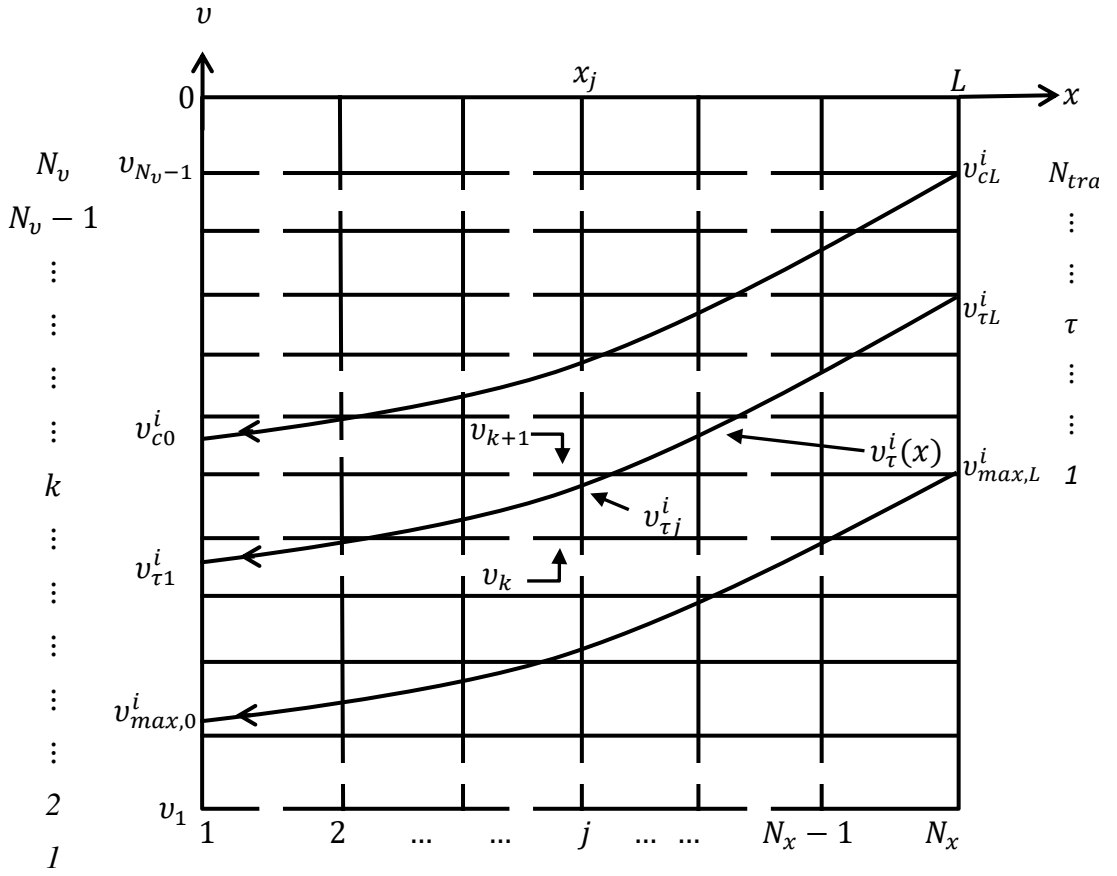


Figure 4.2: Schematic representation of the phase-space grid. The vertical and horizontal dashed lines represent the position and velocity grids respectively [30].

Putting the value of 'a' in Eq. (4.32)

$$Q_{j+1} = Q_j + [Q_j - Q_{j-1} + b(\Delta)^2] \quad (4.34)$$

Solving above equation we get,

$$b = \left(\frac{Q_{j+1} + Q_{j-1} - 2Q_j}{2(\Delta x)^2} \right) \quad (4.35)$$

Using this value of 'b' we get the value of 'a' as

$$a = \left(\frac{Q_{j+1} - Q_{j-1}}{2\Delta x} \right) \quad (4.36)$$

Putting the value of 'a' and 'b' in Eq. (3.30)

$$Q(x) = Q_j + (x - x_j) \left(\frac{Q_{j+1} - Q_{j-1}}{2\Delta x} \right) + \frac{1}{2} (x - x_j)^2 \left(\frac{Q_{j+1} + Q_{j-1} - 2Q_j}{(\Delta x)^2} \right) \quad (4.37)$$

from which the first and second derivatives of any quantity $Q(x)$ are approximated as

$$\left(\frac{dQ}{dx} \right)_j = \left(\frac{Q_{j+1} - Q_{j-1}}{2\Delta x} \right) \quad (4.38)$$

and

$$\left(\frac{d^2Q}{dx^2} \right)_j = \left(\frac{Q_{j+1} - Q_{j-1} - 2Q_j}{(\Delta x)^2} \right) \quad (4.39)$$

respectively.

4.6 Electron Density Distribution

The electron density at any grid point x_j is obtained by using the electron distribution function Eq. (4.6) in the expression for particle density Eq. (4.11). In order to obtain the electron density profile we require $\phi(x)$ to be known. In our calculation, we obtain the electron density at the grid point x_j in terms of potential as

$$n_j^e = n_L^e = \exp\left(\frac{e\phi_j}{kT_f^e}\right) \left[1 + \operatorname{erf} \sqrt{\frac{e(\phi_j - \phi_0)}{kT_f^e}} \right] \quad (4.40)$$

Where $n_j^e = n^e(x_j)$ and $\phi_j = \phi(x_j)$. Hence, one can obtain the electron density at any point if potential profile is known.

4.7 Discretizing Ion Velocity Space with a Fixed Grid

As in the Fig. 4.2, the ion velocity space is discretized uniformly, the k^{th} ion velocity grid value being denoted as v_k ($k = 1, 2, 3, \dots, n_v$ with n_v the total number of velocity grid points). In our discretization $k = 1$ and $k = n_v$ correspond to the fastest and the slowest ion velocities respectively. Since in our simulation scheme only ions

with negative velocities are considered, we set $v_{n_i} = 0$ and choose $|n_1|$ sufficiently large such that the velocity of the fastest ion reaching the left-hand boundary does not exceed this value, i.e. $|v_1| \geq |v_{max,o}^i|$. In our case we choose n_v to be large enough for the velocity grid size to be always considerably less than the ion thermal velocity, v_{tf}^i .

4.8 Ion Trajectories

(a) Discrete Set of the Injection Velocities

The ions are injected at the right-hand boundary, $x = L$, in the velocity range $-\infty < v \leq v_{cL}^i$. In our numerical implementation, we approximate this domain by the finite $v_{max,L}^i \leq v \leq v_{cL}^i$ and discretize the latter with n_{tra} equidistant ion injection velocities $v_{max,L}^i$ and v_{cL}^i respectively. Choice of v_{cL}^i depends on the problem considered and the maximum injection velocity, $v_{max,L}^i$, is chosen sufficiently large for the ion distribution function corresponding to velocities larger than this velocity to be negligible. In our computations, we use $v_{max,L}^i = v_{cL}^i - 4v_{tf}^i$, where v_{tf}^i is the ion thermal velocity.

(b) Discrete Set of Ion Trajectories

The injection velocity at right-hand boundary, $x = L$, represents the starting velocity of a collisionless ion trajectory the n_{tra} discrete injection velocities $v_{\tau L}^i$, define n_{tra} related trajectories labeled by the index ' τ '. We denote the trajectory corresponding to some injection velocity v_{cL}^i by $v_{\tau}^i(L)$, and the velocity with which it crosses a grid point x_j is $v_{\tau j}^i = v_{\tau}^i(x_j)$, so that $v_{\tau n_x}^i \equiv v_{\tau L}^i = v_{\tau}^i(L)$ in phase space. The velocities v_{τ}^i , represent the intersections of ion trajectories $v = v_{\tau}^i(L)$ and the velocity with which it crosses a grid point $x = x_j$, $v_{\tau j}^i = v_{\tau}^i(x_j)$, which is said to be "intersection velocities". The ion injection velocities, $v_{\tau L}^i$, are independent of the ion grid velocities v_k , but in practice we will often choose them such that each $v_{\tau L}^i$ coincide with one of the v_k 's.

(c) Numerical Calculation of Ion Trajectories

In the KTS method, we trace the collisionless trajectories to calculate the related velocity distribution functions along them. In this section, we consider only ion trajectories and hence omit the species index ' i '. For the calculation of the ion

trajectory, we simply discretize the ion equations of motion (4.14), (4.15) and (4.17) in a time-centred manner as

$$\frac{x^{m+\frac{1}{2}}-x^{m-\frac{1}{2}}}{\Delta t} = v_x^m \quad (4.41)$$

and for change in v_x

$$\begin{aligned} \frac{v_x^m - v_x^{m-1}}{\Delta t} &= a_x^{m-\frac{1}{2}} \\ &= \frac{e}{m^i} \left[E \left(x^{m-\frac{1}{2}} \right) + (v \times B)_x^{m-\frac{1}{2}} \right] \\ \frac{v_x^m - v_x^{m-1}}{\Delta t} &= \frac{e}{m^i} E \left(x^{m-\frac{1}{2}} \right) - \frac{e B_0 \sin \theta}{m^i} v_z^{m-\frac{1}{2}} \end{aligned} \quad (4.42)$$

For change in v_y

$$\begin{aligned} \frac{v_y^m - v_y^{m-1}}{\Delta t} &= a_y^{m-\frac{1}{2}} \\ &= \frac{e}{m^i} \left[0 + (v \times B)_y^{m-\frac{1}{2}} \right] \\ \frac{v_y^m - v_y^{m-1}}{\Delta t} &= \frac{e B_0 \cos \theta}{m^i} v_z^{m-\frac{1}{2}} \end{aligned} \quad (4.43)$$

For change in v_z

$$\begin{aligned} \frac{v_z^m - v_z^{m-1}}{\Delta t} &= a_z^{m-\frac{1}{2}} \\ &= \frac{e}{m^i} \left[0 + (v \times B)_z^{m-\frac{1}{2}} \right] \\ \frac{v_z^m - v_z^{m-1}}{\Delta t} &= \frac{e B_0}{m^i} \left(v_x^{m-\frac{1}{2}} \sin \theta - v_y^{m-\frac{1}{2}} \cos \theta \right) \end{aligned} \quad (4.44)$$

respectively, where Δt is the numerical time-step size, $m \geq 0$ is an integer such that the integral or half integral superscript $m \geq 0$ is such that $v^m = v(t^m)$, $x^{m+\frac{1}{2}} = x \left(t^{m+\frac{1}{2}} \right)$ etc. This corresponds to the total time elapsed in steps of Δt for an ion having been injected at time zero at the right-hand boundary. So, $m = 0$ corresponds to $t = 0$ with the injection (or starting) values.

$$x^0 = L \quad (4.45)$$

and

$$v^0 = v_{\tau L}^i \quad (4.46)$$

The choice of positions at half integral times and velocity at integral times in Eq. (4.41), Eq. (4.42), Eq.(4.43) and Eq. (4.44) makes the numerical scheme time-centred. For any time step $m \geq 1$, with $x^{m-\frac{1}{2}}$ and v^{m-1} being given from the $(m-1)^{st}$ step, we calculate the new ion velocity from Eq. (4.42) as

$$v^m = v^{m-1} + \frac{e\Delta t}{m^i} E(x^{m-\frac{1}{2}}) \quad (4.47)$$

and we can also find new position of the ions from Eq. (3.41)

$$x^{m+\frac{1}{2}} = x^{m-\frac{1}{2}} + \Delta t v^m \quad (4.48)$$

Thus, the numerical scheme ends up with x -points at half-integral time $(x^{m+\frac{1}{2}})$ and velocities at integral time (v^m) along a collisionless trajectory. We can also find the ion velocity at $x^{m+\frac{1}{2}}$ by the relation

$$\frac{v^m + v^{m+1}}{2} = v^{m+\frac{1}{2}} \quad (4.49)$$

(d) Intersection Velocities

The velocities at half integral time as in Eq. (4.49) may not coincide with our fixed grid points x_j . For the calculation of the intersection velocities for the τ^{th} trajectory at some inner grid point, x_j , the linear interpolation can be used as

$$v_{\tau j}^i = \frac{\left(x^{m-\frac{1}{2}} - x_j\right)v^{m+\frac{1}{2}} + \left(x_j - x^{m-\frac{1}{2}}\right)v^{m-\frac{1}{2}}}{\left(x^{m-\frac{1}{2}} - x^{m+\frac{1}{2}}\right)} \quad (4.50)$$

Where, $x^{m-\frac{1}{2}}$ and $x^{m+\frac{1}{2}}$ are the adjacent points along the trajectory on the right and the left-hand side of the grid point x_j , respectively. In order to calculate the ion velocity at the left-hand boundary ($x = 0$) we use a parabolic extrapolation scheme. For this, considering the last three calculated points along the trajectory which lie to the right-hand side of the left-hand boundary

$\left[\left(x^{m-\frac{1}{2}}, v^{m-\frac{1}{2}} \right), \left(x^{m-\frac{3}{2}}, v^{m-\frac{3}{2}} \right) \text{ and } \left(x^{m-\frac{5}{2}}, v^{m-\frac{5}{2}} \right) \right]$, the ion velocity near the left-hand boundary is approximated as

$$v(x) = v^{m-\frac{5}{2}} + a \left(x - x^{m-\frac{5}{2}} \right) + b \left(x - x^{m-\frac{5}{2}} \right)^2 \quad (4.51)$$

where 'a' and 'b' are constants. The value of the constants are calculated and at the point $x = x^{m-\frac{1}{2}}$, the velocity is approximated as

$$v^{m-\frac{1}{2}} = v^{m-\frac{5}{2}} + a \left(x^{m-\frac{1}{2}} - x^{m-\frac{5}{2}} \right) + b \left(x^{m-\frac{1}{2}} - x^{m-\frac{5}{2}} \right)^2 \quad (4.52)$$

$$a = \frac{v^{m-\frac{1}{2}} + v^{m-\frac{5}{2}} - b \left(x^{m-\frac{1}{2}} - x^{m-\frac{5}{2}} \right)^2}{\left(x^{m-\frac{1}{2}} - x^{m-\frac{5}{2}} \right)} \quad (4.53)$$

at the point $x = x^{m-\frac{3}{2}}$ the velocity is approximated as

$$v^{m-\frac{3}{2}} = v^{m-\frac{5}{2}} + a \left(x^{m-\frac{3}{2}} - x^{m-\frac{5}{2}} \right) + b \left(x^{m-\frac{3}{2}} - x^{m-\frac{5}{2}} \right)^2 \quad (4.54)$$

using the value 'a' from Eq. (4.53) in Eq. (4.54), we obtain

$$v^{m-\frac{3}{2}} = v^{m-\frac{5}{2}} + \left[\frac{v^{m-\frac{1}{2}} - v^{m-\frac{5}{2}} - b \left(x^{m-\frac{1}{2}} - x^{m-\frac{5}{2}} \right)^2}{\left(x^{m-\frac{1}{2}} - x^{m-\frac{5}{2}} \right)} \right] \left(x^{m-\frac{3}{2}} - x^{m-\frac{5}{2}} \right) + b \left(x^{m-\frac{3}{2}} - x^{m-\frac{5}{2}} \right)^2 \quad (4.55)$$

Then from above equation, we obtain the value of 'b' as

$$b = \frac{\left(x^{m-\frac{5}{2}} - x^{m-\frac{3}{2}} \right) \left(v^{m-\frac{1}{2}} - v^{m-\frac{5}{2}} \right) - \left(x^{m-\frac{5}{2}} - v^{m-\frac{1}{2}} \right) \left(v^{m-\frac{3}{2}} - v^{m-\frac{5}{2}} \right)}{\left(x^{m-\frac{5}{2}} - x^{m-\frac{1}{2}} \right) \left(x^{m-\frac{5}{2}} - x^{m-\frac{3}{2}} \right) \left(x^{m-\frac{3}{2}} - x^{m-\frac{1}{2}} \right)} \quad (4.56)$$

using this value of 'b' in Eq. (4.53), the value of 'a' is obtained as

$$a = \frac{\left(x^{m-\frac{5}{2}} - x^{m-\frac{3}{2}} \right)^2 \left(v^{m-\frac{1}{2}} - v^{m-\frac{5}{2}} \right) - \left(x^{m-\frac{5}{2}} - x^{m-\frac{1}{2}} \right)^2 \left(v^{m-\frac{3}{2}} - v^{m-\frac{5}{2}} \right)}{\left(x^{m-\frac{5}{2}} - x^{m-\frac{1}{2}} \right) \left(x^{m-\frac{5}{2}} - x^{m-\frac{3}{2}} \right) \left(x^{m-\frac{3}{2}} - x^{m-\frac{1}{2}} \right)} \quad (4.57)$$

Then using the value of constants 'a' and 'b' from Eq. (4.56) and Eq. (4.57) onto the Eq. (4.50), the ion velocity at the left-hand boundary is calculated as

$$v_{\tau}^i(x=0) = v^{m-\frac{5}{2}} - ax^{m-\frac{5}{2}} + b \left(x^{m-\frac{5}{2}} \right)^2 \quad (4.58)$$

4.9 Ion Velocity Distribution Function

When we trace the ion trajectories for all n_{tra} injection velocities $v_{\tau L}^i$, we can calculate the corresponding intersection velocities Eq. (4.50) and the related distribution functions at all grid point x_j . The injection velocity from where we start are usually uniformly spaced, but, the corresponding ion velocities at the other grid points, $0 \leq x_j < L$, are non-uniformly spaced and usually do not coincide with the fixed grid velocities, v_k . For our $1d3v$ model, it is not necessary to know the ion distribution function at these uniformly spaced grid velocities.

We can calculate the ion distribution function at the fixed grid points (position and velocity) by inner interpolation of the value associated with the trajectory intersection points to the nearest desired grid points.

4.10 Ion Density Distribution

The ion density distribution, $n^i(x)$, is obtained from the following two approaches:

(a) Distribution-Function Approach (DFA)

In the DFA, the ion density $n^i(x_j)$ is obtained by integrating the ion velocity distribution function over velocity space. For the plasma model we have chosen, we obtain the ion distribution function only at the intersection points $[x_j, v_{\tau}^i(x_j)]$ and can also be obtained at the fixed grid point $[x_j, v_k]$ where the distribution function is given. The ion density at x_j , where the distribution functions, $f^i(x_j, v_{\tau j}^i)$, and the intersection velocities of all n_{tra} ion trajectories, $v_{\tau j}^i$, are given, may be obtained by the following discretized from

$$n^i(x_j) = \frac{1}{2} \sum_{\tau=1}^{n_{tra}-1} [f^i(x_j, v_{\tau j}^i) + f^i(x_j, v_{\tau+1,j}^i)] (v_{\tau+1,j}^i - v_{\tau j}^i) \quad (4.59)$$

$$n^i(L) = \frac{1}{2} \sum_{\tau=1}^{n_{tra}-1} [f^i(L, v_{\tau j}^i) + f^i(L, v_{\tau+1,j,L}^i)] (v_{\tau+1,L}^i - v_{\tau j}^i) \quad (4.60)$$

4.11 Solution of Poisson's Equation

After the calculation of the electron and ion densities from Eq. (4.40) and Eq. (4.60), the space charge density distribution can be obtained using

$$\begin{aligned}
\rho(x_j) &= \sum q^s n^s(x_j) \\
&= e[n^i(x_j) - n^e(x_j)]
\end{aligned} \tag{4.61}$$

By the knowledge of the space charge distribution, $\rho(x_j)$, from Eq. (3.22) we can solve the Poisson's Eq. (3.21) numerically to obtain the related new potential distribution, $\phi(x_j)$, Using Eq. (4.39), the discretized form of Poisson's equation is given by

$$\frac{\phi_{j+1} - 2\phi_j + \phi_{j-1}}{(\Delta x)^2} = -\frac{\rho_j}{\epsilon_0} \tag{4.62}$$

Now we write this equation for all internal grid points in the simulation region $j = 2, 3, \dots, \dots, n_x - 1$ which yields the following $n_x - 2$ equations involving n_x unknowns, $\phi_1, \phi_2, \dots, \phi_{n_x}$:

$$\phi_1 - 2\phi_2 + \phi_3 = -\frac{(\Delta x)^2}{\epsilon_0} \rho_2 \tag{4.63}$$

$$\phi_2 - 2\phi_3 + \phi_4 = -\frac{(\Delta x)^2}{\epsilon_0} \rho_2$$

$$\phi_{n_x-2} - 2\phi_{n_x-1} + \phi_{n_x} = -\frac{(\Delta x)^2}{\epsilon_0} \rho_{n_x-1}$$

We have fixed the potential values at the two boundaries as

$$\begin{aligned}
\phi(x = L) &= \phi_{n_x} \\
&= \phi_L
\end{aligned} \tag{4.64}$$

and

$$\begin{aligned}
\phi(x = 0) &= \phi_1 \\
&= \phi_0
\end{aligned} \tag{4.65}$$

By solving the Eq. (4.63), Eq. (4.64) and Eq. (4.65) we now obtain the potential distribution, i.e. the potential values $\phi_1, \phi_2, \dots, \phi_{n_x}$ which can be expressed as a single matrix equations as,

$$\begin{pmatrix} 1 & 0 & 0 & 0 & \cdot & \cdot & 0 \\ 1 & -2 & 1 & 0 & \cdot & \cdot & 0 \\ 0 & 1 & -2 & \cdot & \cdot & \cdot & 0 \\ \cdot & \cdot & \cdot & \cdot & \cdot & \cdot & \cdot \\ \cdot & \cdot & \cdot & \cdot & \cdot & \cdot & \cdot \\ \cdot & \cdot & \cdot & \cdot & 1 & -2 & 1 \\ \cdot & \cdot & \cdot & \cdot & 0 & 0 & 1 \end{pmatrix} \times \begin{pmatrix} \phi_1 \\ \phi_2 \\ \vdots \\ \phi_{n_x-1} \\ \phi_{n_x} \end{pmatrix} = \begin{pmatrix} \phi_0 \\ -\frac{(\Delta x)^2}{\epsilon_0} \rho_2 \\ \vdots \\ -\frac{(\Delta x)^2}{\epsilon_0} \rho_{n_x-1} \\ \phi_L \end{pmatrix} \quad (4.66)$$

The matrix on the left-hand side and the one at the right-hand side are known. In order to solve the matrix equation inverse of the first matrix is multiplied with the right-hand side matrix which is done using a simple command in MATLAB program.

4.12 Relaxation Scheme

The exact solution of Poisson's equation converges only for short systems (a few Debye lengths). As the system length increase, small fluctuation of the potential causes unphysical accumulation of the charges and the scheme breaks down. To overcome this difficulty we use the relaxation scheme [35]. The numerically exact potential distribution function $\phi_{ex}^{(m)}$ obtained by numerically solving Eq. (4.66) is linearly combined with old potential distribution $\phi^{(m-1)}(x_j)$ to obtain the "re-adjusted" new potential distribution function $\phi^{(m)}(x_j)$, which is actually used as the relevant result of the m^{th} iteration:

$$\phi^{(m)}(x_j) = \omega \phi_{ex}^{(m)} + (1 - \omega) \phi^{(m-1)}(x_j) \quad (4.67)$$

with $0 < \omega < 2$.

4.13 Iteration Scheme

We are dealing with collisionless, time independent system only. The initial-guess potential, $\phi^{(0)}(x_j)$, is taken as input to the main iteration block (located between the points A and B in Fig. 4.3, which will yield the first iteration to the potential distribution $\phi^{(1)}(x_j)$. With the new potential as input, the main iteration block will be invoked again yielding $\phi^{(2)}(x_j)$ until the potential distribution has converged in the sense outlined in Sec. 4.14 below.

(a) Boundary Conditions:

The boundary potentials, $\phi(0)$ and $\phi(x = L)$, and the boundary injection distribution functions, $f^s(L, v)$, are to be provided as input parameters. Hence, they must be specified before entering the iteration scheme and are kept constant throughout the entire simulation.

(b) Initial guess to $\phi(x)$:

To start the scheme, we must suitably prescribe an initial-guess potential distribution. As we restrict ourselves to potential distributions $\phi(x)$, which decrease monotonically from $\phi(L) = 0$ to $\phi(0) = \phi_0 < 0$. The starting potential distribution is chosen to be a linear interpolation between the potential values at the boundaries.

4.14 Main Iteration Block

Here we describe the main iteration scheme discussed in the Fig. 4.3. The main iteration block carries out the m^{th} iteration (i.e. it calculates the new distributions, $\phi^m(x_j)$ for a given input (old) potential distribution, $\phi^{m-1}(x_j)$, by performing the following three steps.

Step 1: The new electron density distribution $n^{e(m)}(x_j)$ is calculated analytically using Eq. (4.40). The new ion density $n^{i(m)}(x_j)$ is calculated by velocity-space integration of the new velocity distribution function [cf. Sec. 4.10(a)].

Step 2: From the new densities, $n^{e(m)}(x_j)$, obtained in step 1, the new space-charge density, $\rho^{(m)}(x_j)$, is calculated using the Eq. (4.16).

Step 3: The new potential distribution, $\phi^{(m)}(x_j)$, is calculated by solving the matrix Eq. (4.66) numerically with the new space-charge density, $\rho^{(m)}(x_j)$, inserted on the right-hand side.

Step 4: The Thomas Fermi reduced energy e is calculated analytically using Eq. (1.6).

Step 5: The ion reflection coefficient R_N is calculated by solving Eq. (1.5).

4.15 Convergence Check

The new potential distribution $\phi^{(m)}(x_j)$, obtained in Step 3 of the main iteration block is compared with the old potential distribution, $\phi^{(m-1)}(x_j)$, and we consider the convergence to be reached if at each point x_j the condition

$$|\phi^{(m)}(x_j) - \phi^{(m-1)}(x_j)| \leq \delta \quad (4.68)$$

is satisfied, where δ is a defined accuracy parameter.

4.16 Ion Reflection Coefficient

The velocity of ions $v_{i\omega}$ at wall is calculated using Eq. (4.58). The kinetic energy is then calculated as

$$E_{ions} = \frac{1}{2} m v_{i\omega}^2 \quad (4.69)$$

The sum of all energies is

$$E_0 = \text{sum}(E_{ions}) \quad (4.70)$$

After calculating E_0 , the Thomas Fermi reduced energy is calculated using Eq. (1.6).

$$\epsilon = 0.0325 \frac{\mu}{\mu+1} \frac{1}{Z_1 Z_2 \left(Z_1^{\frac{2}{3}} + Z_2^{\frac{2}{3}} \right)^{\frac{1}{2}}} E_0 \quad (4.71)$$

And ion reflection coefficient is obtained by using Eq. (1.5)

$$R_N = \frac{A_1 \ln(A_2 \epsilon + e)}{1 + A_3 \epsilon^{A_4} + A_5 \epsilon^{A_6}} \quad (4.72)$$

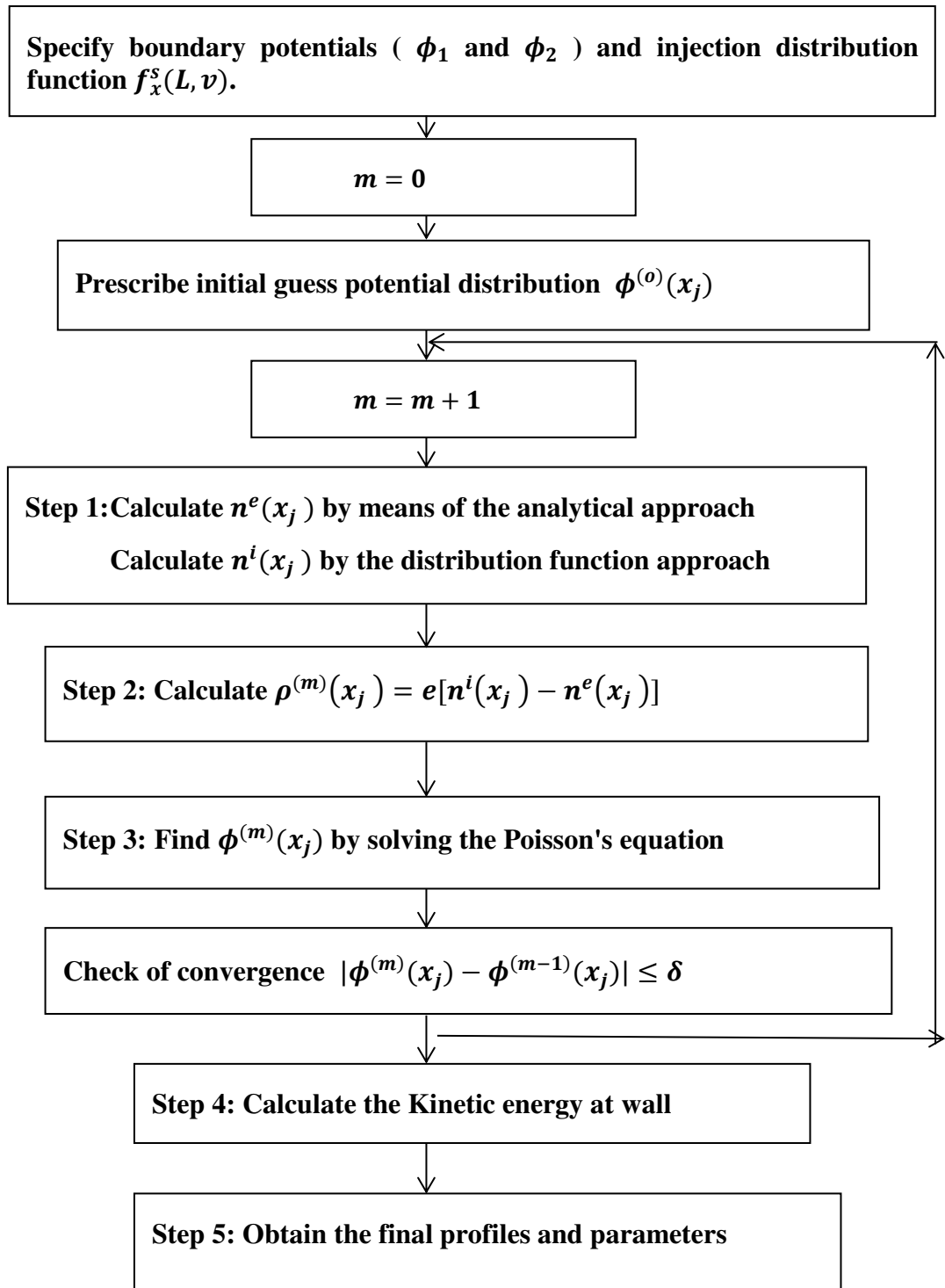


Figure 4.3: The flowchart showing Iteration scheme.

4.17 Numerical Parameters

We are using Kinetic Trajectory Simulation approach to a plasma sheath model, considering the parameters at the presheath side of the sheath-presheath boundary to be given. As we are dealing with both deuterium and tritium plasmas we are considering the following parameters at the presheath side of the sheath-presheath boundary.

- (i) deuterium and tritium plasma with their respective mass and charge but with the same plasma density, $n_{ps} = 10^{18} m^{-3}$.
- (ii) electron temperature is taken to be constant at 4eV.
- (iii) sheath width is taken as 10 times the electron debye length i.e. $10\lambda_D^e$.
- (iv) ion temperature is varied from 0.5 eV to 2.5 eV.

The dimensional sheath parameters at the sheath side of the sheath-presheath boundary can then be obtained from the coupling scheme. At the sheath entrance the ion injection velocities are discretized uniformly with 300 injection velocity grid points in such a way that the ion injection velocity grid step is considerably less than the thermal velocity of ions. The region between $x=0$ to $x=L$ is discretized uniformly with 31 grid points and if the maximum difference in potential values before and after iteration equals 10^{-7} V or less then we consider the system to have reached the convergence.

Chapter 5

Results and Discussion

5.1 Ion Reflection Coefficient

The respective ion reflection coefficient by carbon and tungsten wall with magnetic field 30 mT at angle 30° for different ion temperatures in the presence of deuterium (D-plasma) and tritium (T-plasma) plasma is shown by figures 5.1 and 5.2. It is observed that ion reflection coefficient by both carbon and tungsten wall decreases with the increase in the ion temperature. Also, ion reflection coefficient by tungsten wall is higher compared to that of carbon wall as the atomic mass of tungsten is much larger. The energy transfer during the elastic collision between the ion and the target nucleus increases as the temperature increases and when it exceeds the threshold value called displacement energy, the target atom leaves its lattice site vacant called vacancy and the ions are absorbed. From this it can be concluded that ion reflection coefficient is energy dependent, higher the projectile energy ions are less likely to be reflected from material wall. Furthermore, ion reflection coefficient in Tritium plasma is comparatively higher than in Deuterium plasma at a given temperature.

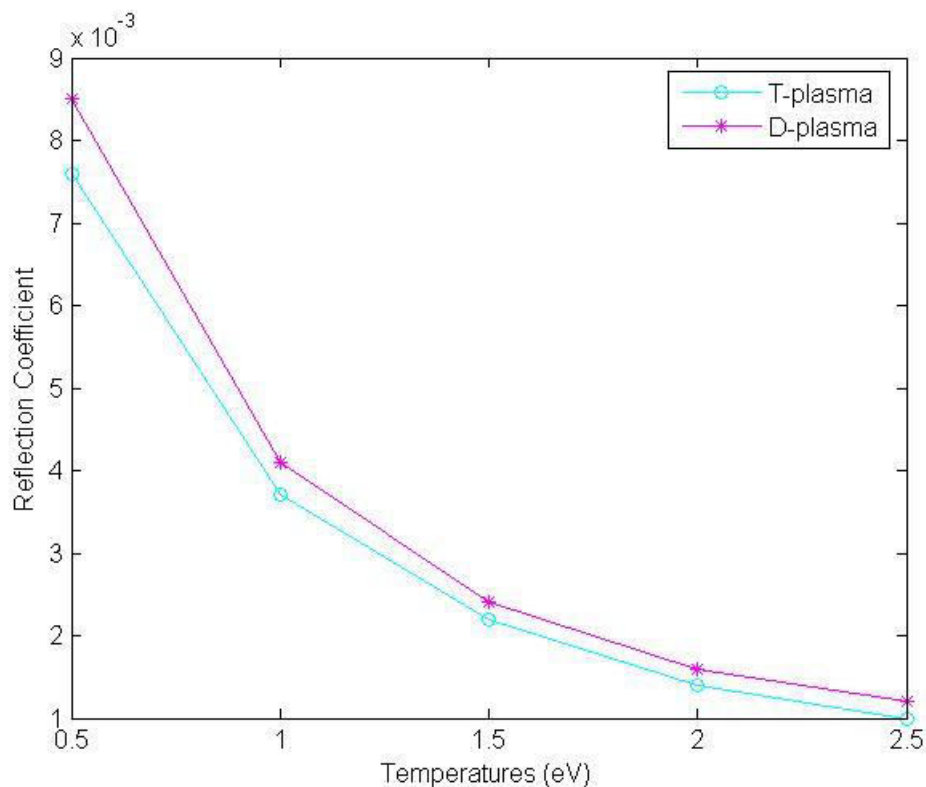


Figure 5.1: Reflection coefficient vs. ion temperature on Carbon wall in D and T plasma.

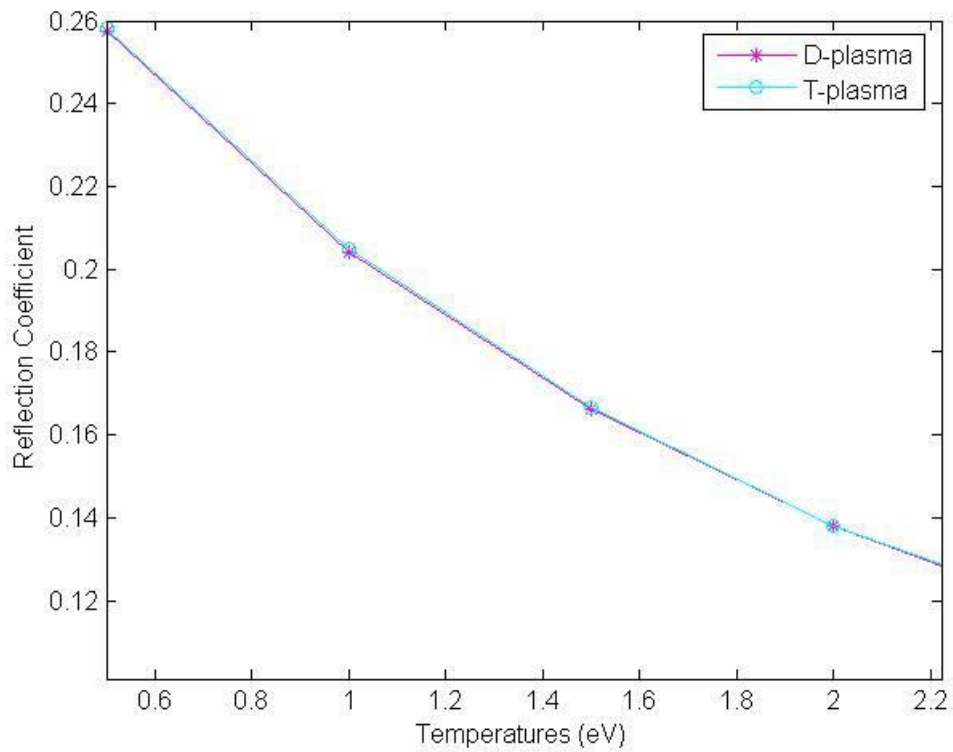


Figure 5.2: Reflection coefficient vs. ion temperature on Tungsten wall in D and T plasma.

5.2 Ion Absorption Coefficient

Figure 5.3 and 5.4 shows the variation of the ion absorption coefficient by the carbon and tungsten wall in the presence of magnetic field of 30 mT at angle 30° in deuterium and tritium plasma for varying ion temperatures. From the figure, it can be observed that the ion absorption coefficient of both carbon and tungsten increases as the ion temperature is increased regardless of the choice of plasma. As the temperature is increased, the energy of the projectile particles is also increased, which leads to the increase in the particle absorption coefficient. Further, it has been observed that that the ion absorption coefficient by tungsten is less compared to that by carbon as it varies with projectile energy, projectile mass and mass of the target atom. It also has been observed that the ion absorption coefficient for carbon and tungsten wall in deuterium plasma is higher than in tritium plasma.

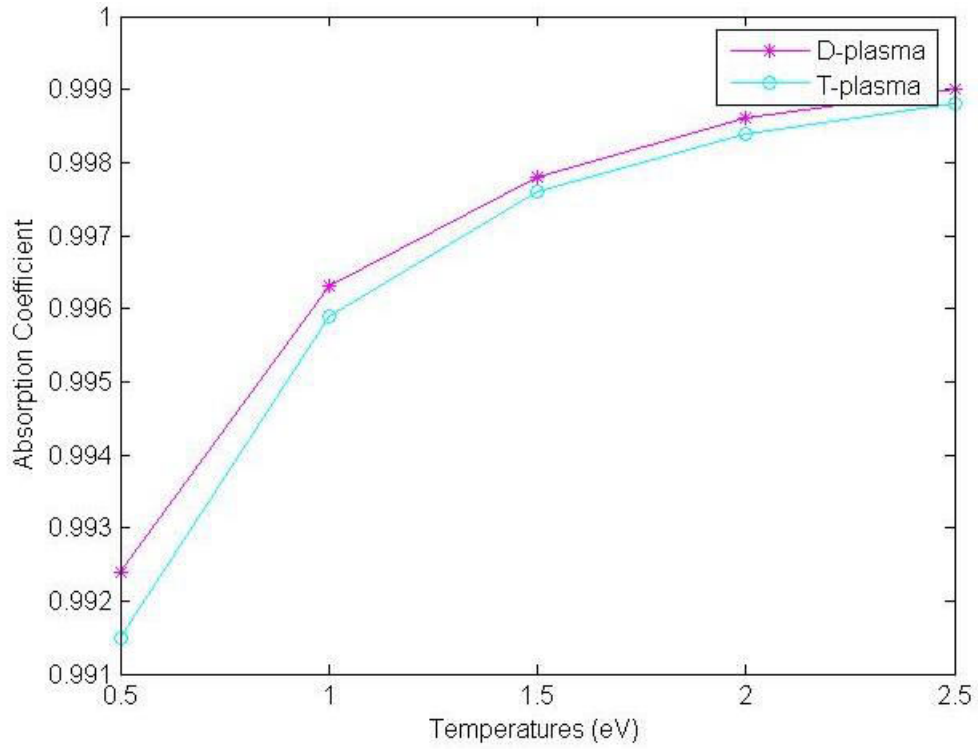


Figure 5.3: Ion absorption coefficient vs. ion temperature on carbon wall in D and T plasma

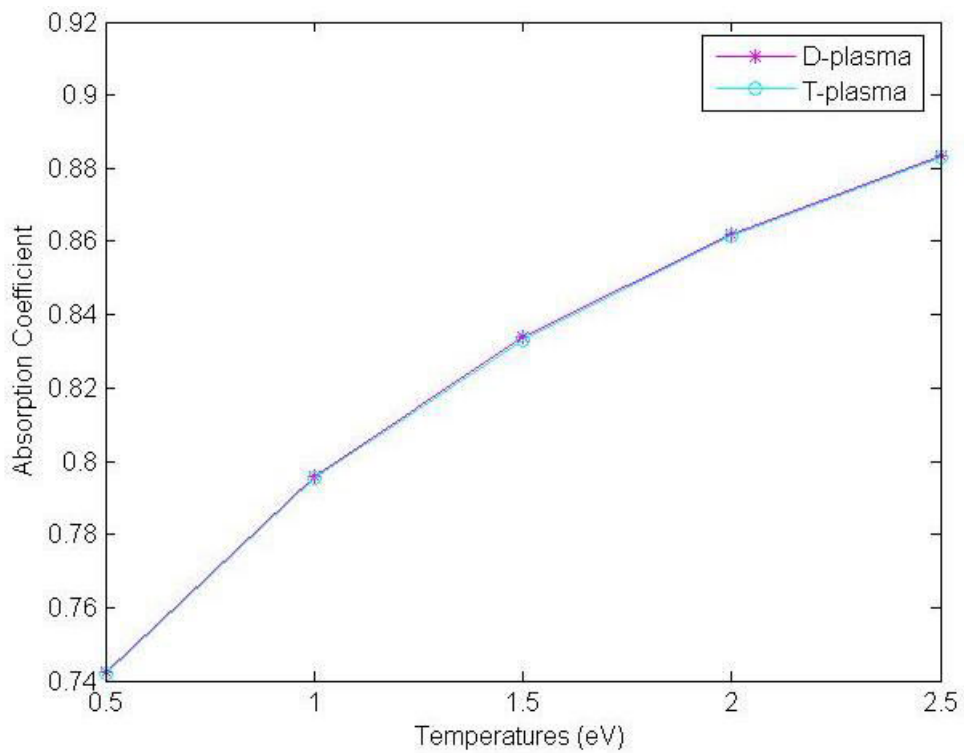


Figure 5.4: Ion absorption coefficient vs. ion temperature on tungsten wall of D and T plasma.

5.3 Reflected Ion Density

Figure 5.5 and 5.6 shows the variation of the reflected ion density by the carbon and tungsten wall in deuterium plasma and tritium plasma for different ion temperatures keeping the remaining parameters fixed. From the figure, it can be clearly observed that the reflected ion density decreases as the temperature is increased. When the temperature increases, the ion reflection coefficient on carbon and tungsten wall also decreases and hence the reflected ion density by wall also decreases. It has been observed that the reflected ion density by tungsten wall is greater than that by carbon wall, since the ion reflection coefficient is not only dependent on the energy of the incident particles but also depends on the mass ratio of the incident particles and the target atom. Also, it has been observed that the ion reflection coefficient by tungsten wall is higher than by carbon wall regardless of the choice of plasma which is due to the higher atomic mass of tungsten. But reflected ion density by tungsten wall in case of tritium plasma is larger compared to the case when deuterium plasma is used, as the mass ratio of tritium plasma to tungsten wall is comparatively higher.

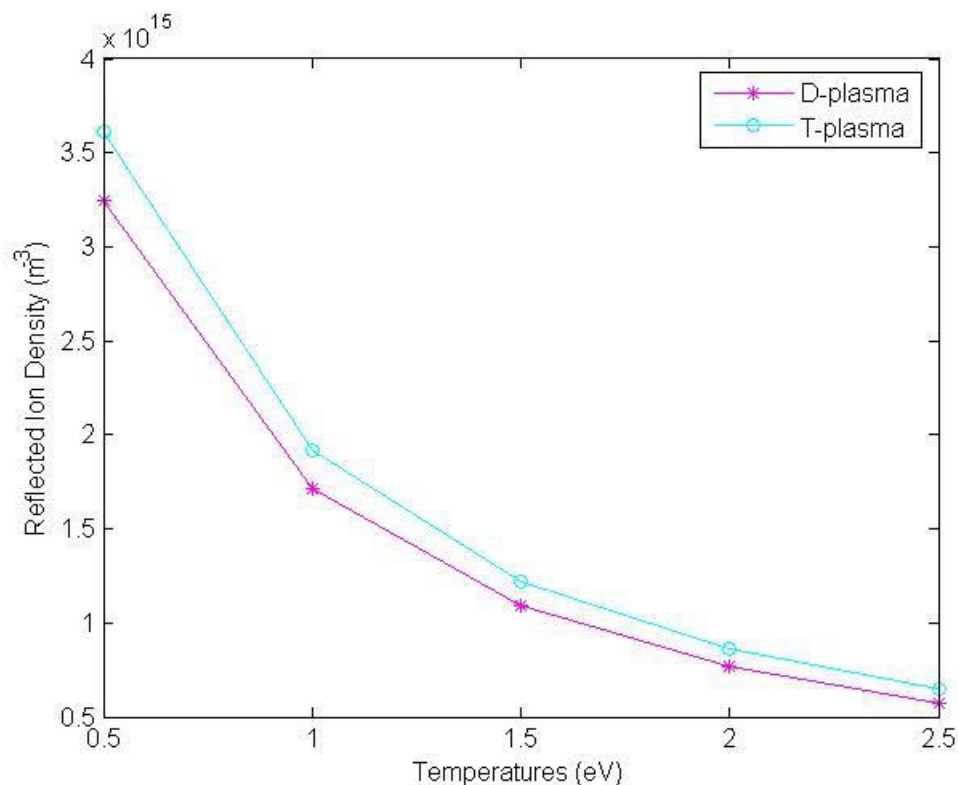


Figure 5.5: Reflected ion density through carbon wall in D and T-plasma for different ion temperatures.

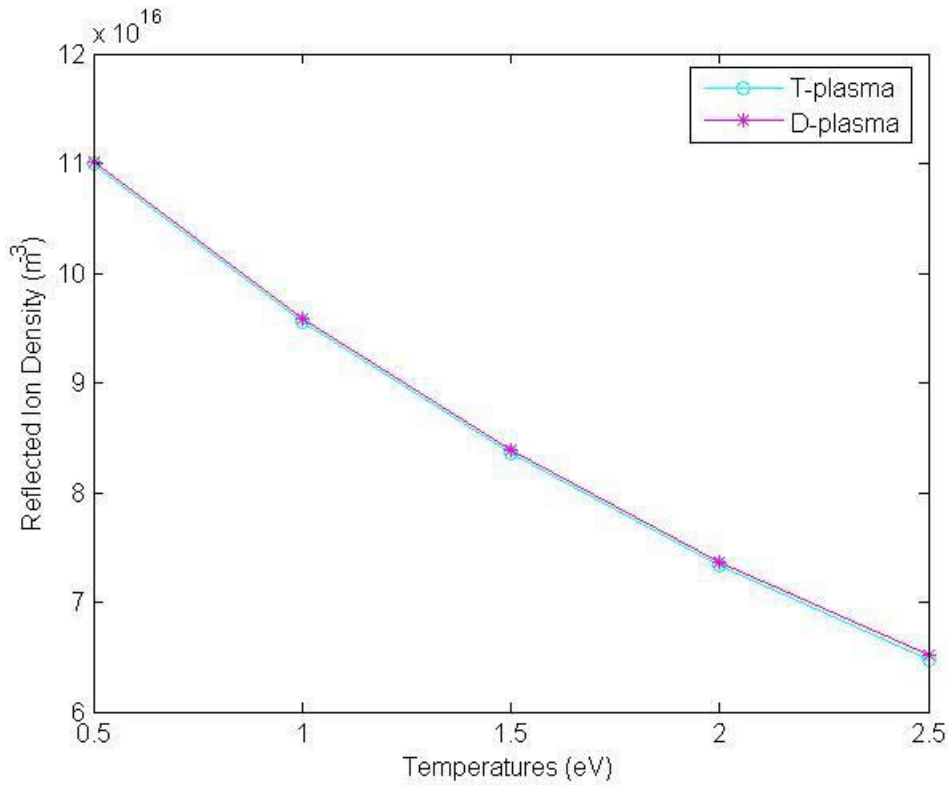


Figure 5.6: Reflected ion density on tungsten wall in D and T-plasma for different ion temperatures.

5.4 Absorbed Ion Density

Figure 5.7 and 5.8 shows the variation of the absorbed ion density on the carbon and tungsten wall with D and T-plasma at different ion temperatures. From the figure it can be clearly observed that the absorbed ion density by carbon and tungsten wall increases as the increase in temperature of ions. As the temperature is increased the thermal velocity of the incident particles is also increased and thus the energy is also increased. Also, it has been observed that the ion absorption by carbon wall is greater than by tungsten wall. It can also be observed that ion absorption by carbon wall in D-plasma is higher compared to T-plasma. Since the ion absorption by the material wall depends on the particle absorption coefficients, projectile energy and mass ratio of the projectile and the target atom.

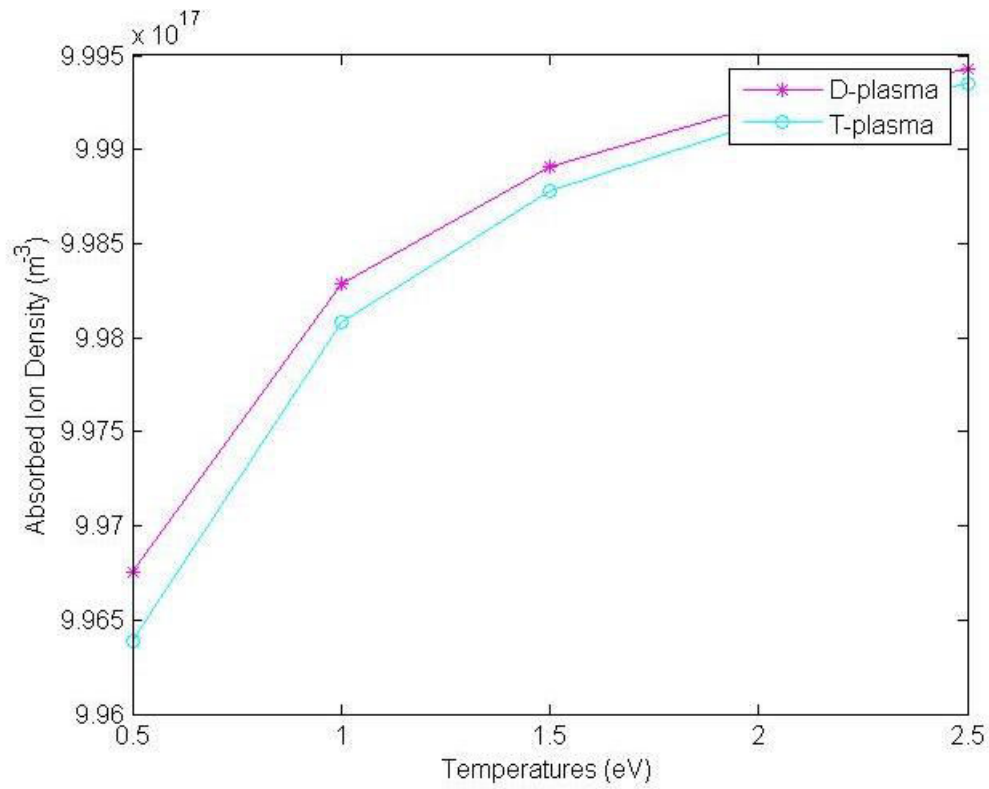


Figure 5.7: Absorbed ion density vs. ion temperature on carbon wall in D and T plasma.

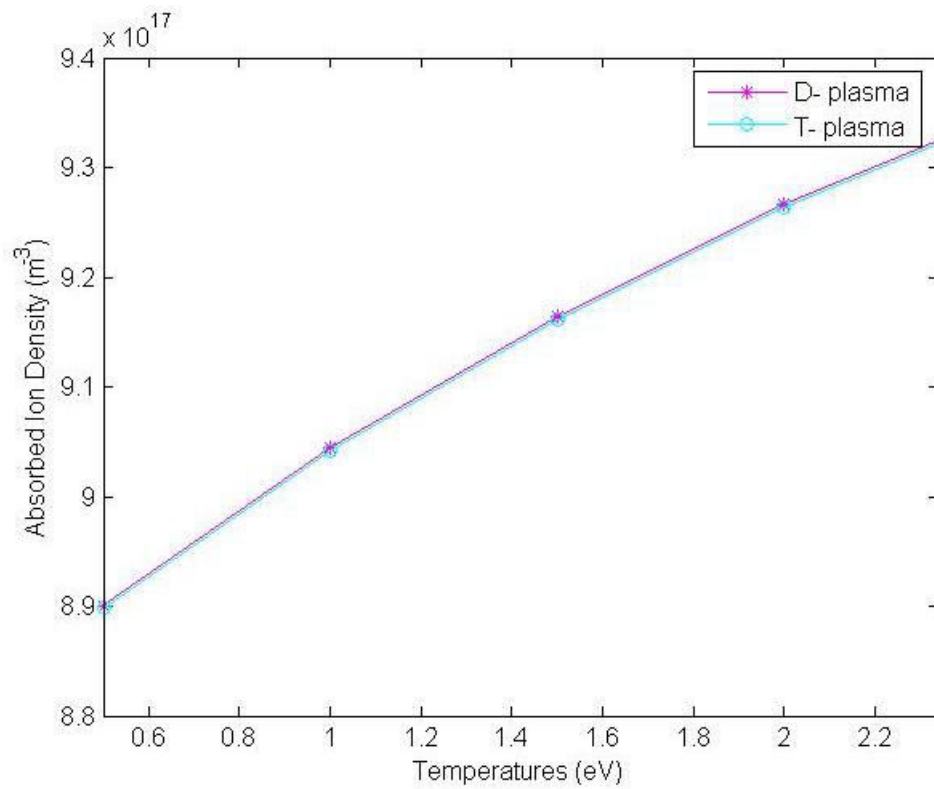


Figure 5.8: Absorbed ion density vs. ion temperature on tungsten wall in deuterium and tritium plasma.

5.5 Total Charge Density

Figure 5.9 and 5.10 shows the distribution of total charge density on the carbon and tungsten wall having different ion temperatures. From the figure, it can be concluded that the total charge density increases with the increase in temperature. The density of both the ion and electron species increases with the increase in temperature and hence the total charge density is increased. The ion reflection coefficient by the tungsten wall is greater than by the carbon wall, thus the density at carbon wall is higher than at tungsten wall. Therefore the total charge density by carbon wall is comparatively higher.

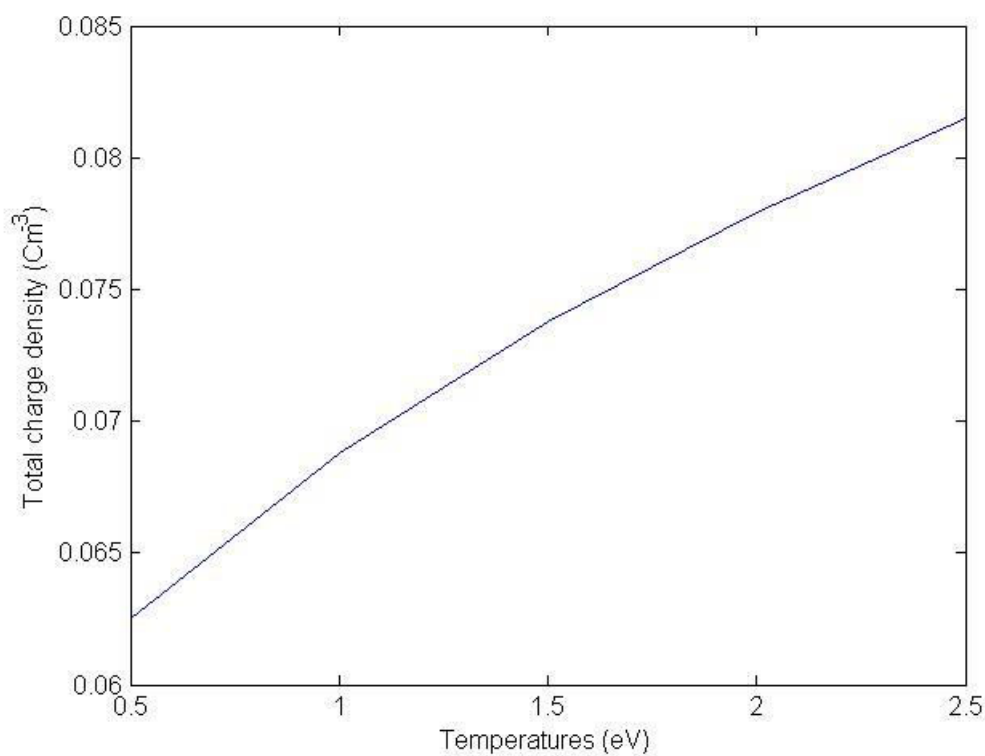


Figure 5.9: Total charge density vs. ion temperature on carbon wall.

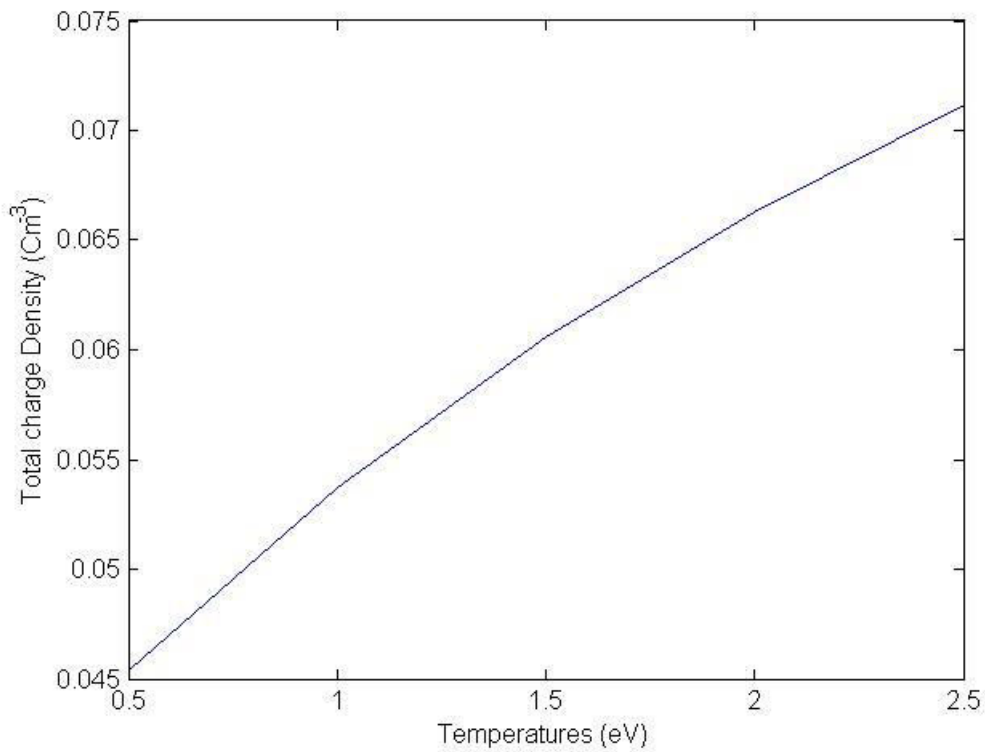


Figure 5.10: Total charge density vs. ion temperature on tungsten wall.

5.6 Thomas Fermi Reduced Energy

Figure 5.11 and 5.12 shows the variation of the Thomas Fermi reduced energy at different temperatures on carbon and tungsten wall in D and T-plasma. From figure it is observed that the Thomas Fermi reduced energy increases linearly with the increase in ion temperature. It can also be observed that Thomas Fermi reduced energy of carbon is higher than that of tungsten for a given ion temperature in a particular fuel component.

It is also clearly observed that the Thomas Fermi reduced energy of carbon and tungsten are comparatively higher in case of D-plasma than in the case of T-plasma at a certain ion temperature and the result is in well agreement with the ion reflection coefficients.

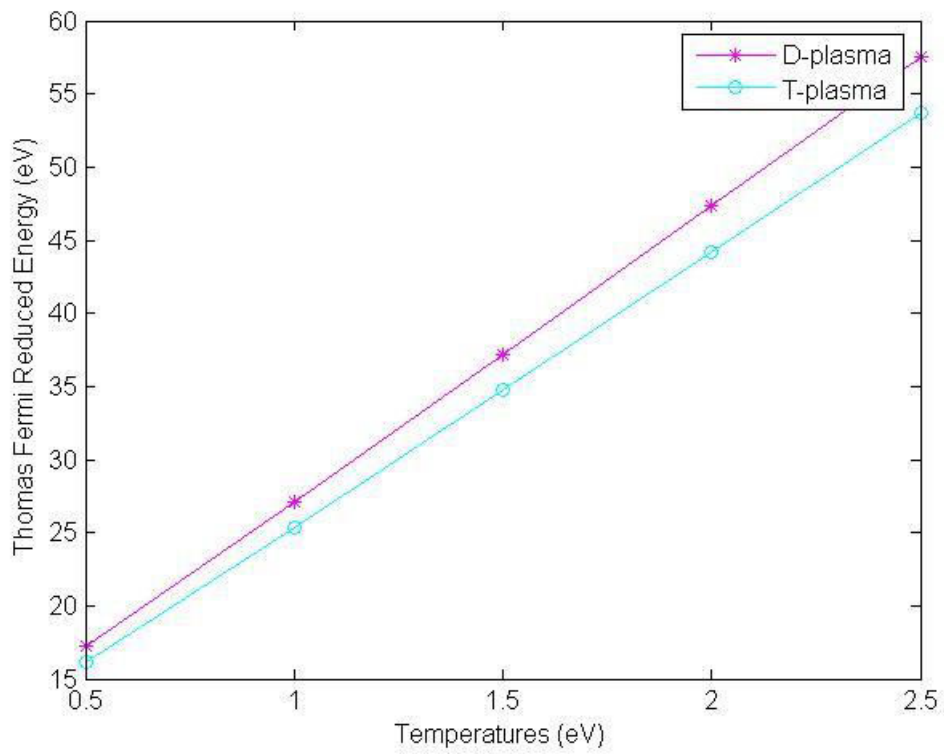


Figure 5.11: Thomas Fermi reduced energy vs. ion temperature on carbon wall in D and T-plasma.

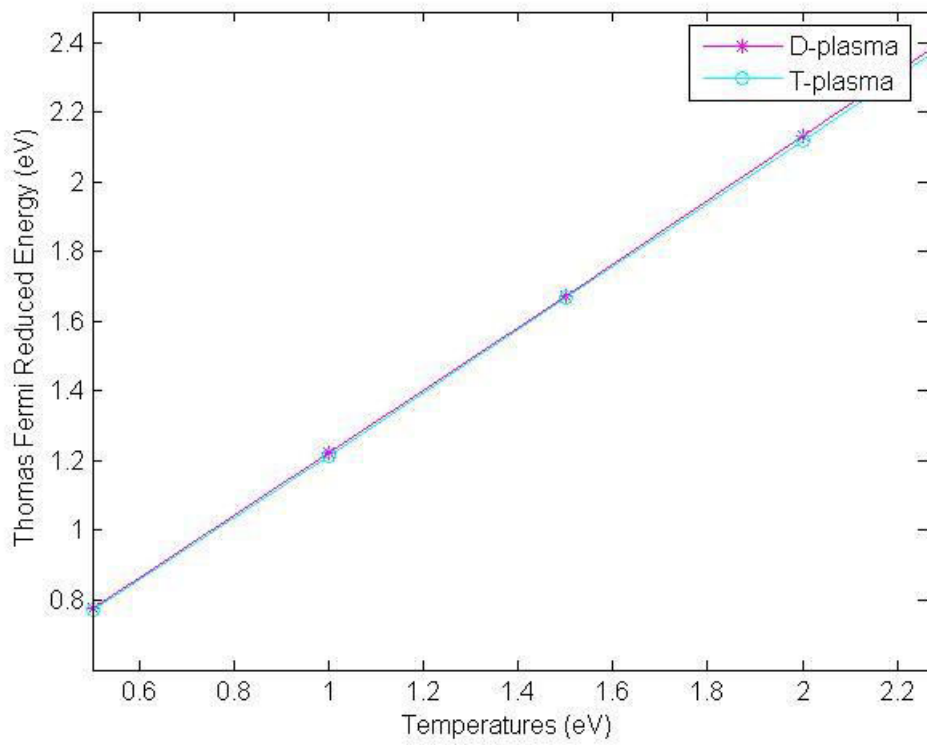


Figure 5.12: Thomas Fermi reduced energy vs. ion temperature on tungsten wall in D and T-plasma.

Chapter 6

Conclusion and Future Works

6.1 Conclusion

We have used Kinetic Trajectory Simulation (KTS) method to study the interaction between plasmas with confining material wall (carbon and tungsten surfaces). We have assumed the plasma with a magnetic field of 30 mT at an orientation of 30° normal to the wall. The electron temperature is kept constant at 4 eV and the ion reflection coefficient, ion absorption coefficient, reflected ion density, absorbed ion density, total charge density and Thomas Fermi reduced energy have been studied.

As the ion temperature is increased, the energy transfer during the elastic collision exceeds the threshold value leaving behind a vacant site and hence ions are absorbed. Thus, absorption of ion increases as we increase the ion temperature and hence the reflection of ion decreases. The reflection coefficient of tungsten is higher than that of carbon in both deuterium and tritium plasmas which is due to the higher mass of tungsten. Also the reflection coefficient of both carbon and tungsten in T-plasma is slightly higher than in D- plasma since the mass ratio of the projectile to the target is also responsible for reflection of ions. For carbon wall the ion reflection coefficient is found to be 0.0076 at 0.5 eV and decreases to 0.0010 at 2.5 eV in D-plasma which slightly increases to 0.0085 and 0.0012 at the respective temperatures. Similarly for tungsten wall the ion reflection coefficient is 0.2576 and 0.1164 in D-plasma but is slightly higher in T-plasma which is found to be 0.2582 and 0.1170 at 0.5 eV and 2.5 eV respectively. The thermal velocity of the projectile particles increases with the increase in temperature which leads to the increase in the ion and electron densities at wall and hence the total charge density of both ions and electrons increases. It is also seen that Thomas Fermi reduced energy also increases linearly with the ion temperature.

This study implies that the ion temperature has significant role in determining the plasma-wall interactions. It also shows the importance of choice of plasma and the confining material surface for applications of plasma where they come into contact with material surfaces.

6.2 Future Works

This study provides a basis for the study of plasma-wall interactions using Kinetic Theory and can be extended further:

- to study the effect of varying electron temperature.
- to study other confining material surfaces like molybdenum, boron, etc.
- to study multicomponent dense plasma.
- to study scattering of ions and electrons in plasmas.

References

- [1] F.F. Chen, *Introduction to Plasma Physics and Controlled Fusion* (third edition), Springer Press, Switzerland (2016).
- [2] R.J. Goldston & P.H. Rutherford, *Introduction to Plasma Physics*, Institute of Physics Publishing, Bristol UK (1995).
- [3] C. Hansen, A.B. Riemann & J. Fajans, *Phys. Plasma* **3**, 1820 (1996).
- [4] K.U. Riemann, *J. Phys. D. Appl. Phys.* **24**, 493 (1991).
- [5] K.U. Riemann, *J. Tech. Phys.* **41**, 89 (2000).
- [6] P.C. Stangeby, *The Plasma Boundary of Magnetic Fusion Devices*, Institute of Physics Publication (2000).
- [7] D. Bohm, *The Characteristics of Electrical Discharges in Magnetic Fields*, Edited by A. Guthry & R. K. Wakerling, McGraw-Hill, New York, 77 (1949).
- [8] R. Chodura, *Phys. Fluids* **25**, 1628 (1982).
- [9] C.A. Ordonez & R.E. Peterjn jr, *J. of Nucl. Materials* **228**, 201 (1996).
- [10] E.W. Thomas, R.K. Janev & J. Smith, *Nucl. Instr. & Meth. in Phys. Res. B* **69**, 452 (1992).
- [11] K. Nagaoka, H. Takahashi, M. Nakata, S. Satake, K. Tanaka, K. Mukai, M. Yokoyama, H. Nakano, S. Murakami, K. Ida, M. Yoshinuma, S. Ohdachi, T. Bando, M. Nunami, R. Seki, H. Yamaguchi, M. Osakabe, T. Morisaki & LHD Experiment Group, *Nucl. Fusion* **59**, 106002 (2019).
- [12] I. Langmuir, *Phys. Rev.* **33**, 954 (1929).
- [13] J.N. Brooks, J.P. Allain, R.P. Doerner, A. Hassanein, R. Nygren, T.D. Rognlien & D.G. Whyte, *Nucl. Fusion* **49**, 035007 (2009).
- [14] R.L.F. Boyd, *Proc. Phys. Soc. B* **64**, 795 (1951).
- [15] A. Cavaliere, F. Engelmann and A. Sestero, *The Phys. of Fluids* **11**, 158 (1968).
- [16] P.C. Stangeby & J.E. Allen, *J. Phys. A: Gen. Phys.* **3**, 304 (1970)
- [17] K.U. Riemann, *Phys. Plasmas* **10**, 3432 (2003).
- [18] K.U. Riemann, *IEEE Trans. Plasma Sci.* **23**, 709 (1995).
- [19] L. Zhengming, H. Qing & T. Lijian, *Nucl. Instr. and Meth. in Phys. Res B* **115**, 505 (1996).
- [20] J.A. Wesson, *Plasma Phys. Control Fusion* **37**, 1459 (1995)
- [21] S. Chauhan, H. K. Malik & R. P. Dahiya, *Phys. of Plasmas* **3**, 3932 (1996)
- [22] E. Ahedo, *Phys. of Plasmas* **4**, 4419 (1997).

- [23] K. Ogawa, M. Isobe, T. Nishitani, R. Seki, H. Nuga, S. Murakami, M. Nakata & L.E. Group, *Plasma Phys. Control. Fusion* **60**, 095010 (2018).
- [24] B. Singha, A. Sarma & J. Chutia, *Pramana- J. Phys.* **55**, 889 (2008).
- [25] R.N. Franklin, *J. Phys. D: Appl. Phys.* **37**, 1342 (2003).
- [26] B.J.B. Crowley, arXiv preprint arXiv: 1508.06101 (2015).
- [27] J. Kawata & K. Ohya, *Japanese J. of Appl. Phys.* **34**, 6237 (1995).
- [28] X. Zhang, B. Shen, M.Y. Yu, X. Li, Z. Jin & F. Wang, *Phys. of Plasmas* **14**, 113108 (2007).
- [29] M. Kaufmann & R. Neu, *Fusion Engineering and Design* **82**, 521 (2007).
- [30] R. Khanal, *A Kinetic Trajectory Simulation Model for Bounded Plasmas*, PhD Thesis, Innsbruck University, Austria (2003).
- [31] R. Chalise, *Study of Magnetized Plasma Wall Transition in an Oblique Magnetic Field*, M.Sc. Dissertation, Tribhuvan University, Kathmandu, Nepal (2011).
- [32] R. Chalise & R. Khanal, *Plasma Phys. Control Fusion.* **54**, 095006 (2012).
- [33] R. Chalise & R. Khanal, *Phys. of Plasma* **22**, 113505 (2015).
- [34] K. Chaudhary, A. M. Imam, S. Z. H. Rizvi & J. Ali, *InTech: Rijeka, Croatia*, 107 (2018).
- [35] W. H. Press, S.A. Teukolsky, B.P. Flannery & W.T. Vetterling, *Numerical Recipes in C*, Cambridge University Press (1989).

Appendix

A MATLAB files

Input

```
% To study the sheath structure for an oblique magnetic field:
Angle =input('Put value of angle made by an oblique magnetic field along x-axis :');
Theta=(Angle*pi/180);    % In terms of radian
% Basic parameters:
B0=-30e-3;                % Applied magnetic field(Tesla)
vy=-2.3045e4;            % Value of Y-component velocity
vz=-2.3045e4;            % Value of Z-component
kB=1.38062e-23;          % Boltzmann constant(J/K)
epsilon=8.85419e-12;     % Permittivity of the medium(F/m)
e=1.602192e-19;         % Electronic charge(C)
Ze=e;                    % Ion charge(C)
Mi=1.672e-27;           % Mass of ion(Kg)
Me=9.109e-31;           % Mass of electron(Kg)
mu=Me/Mi;                % Ratio of Electron to ion mass used in coupling scheme
gammai=3;                % Polytropic constant ions(Isothermal case only)
z1=1;                    % charge of hydrogen ion
m1=2.014;                % mass of deuterium atom
z2c=6;                   % charge of carbon nucleus
z2w=74;                  % charge of tungsten nucleus
m2c=12;                  % mass of carbon nucleus
m2w=183.92;              % mass of tungsten nucleus
% presheath parameters:
```

```

Jps=1; % Total current density at presheath side
Tpse=4*11604.5; % Electron temperature at presheath side(k)
Tpsi=0.25*Tpse; % Ion temperature at presheath side(k)
nps=1e18; % Plasma density at presheath side(1/m^3)
cps=sqrt(kB*(Tpse+gammai*Tpsi)/Mi); % Ion acoustic velocity at presheath(m/s)
upsi=-cps; % Average fluid velocity along x-axis(S.E singularity condition)(m/s)
% Normalized quantities:
JpsN=Jps/e/nps*sqrt(Mi/2/kB/Tpse); % Normalized current density
TpsiN=Tpsi/Tpse; % Normalized ion temperature
upsiN=upsi/sqrt(2*kB*Tpse/Mi); % Normalized average fluid velocity
% sheath parameters:
JL=Jps; % Total current density at x=L(sheath entrance)
phiL=0; % Potential at x=L(sheath entrance)
rhoL=0; % Total charge density at x=L(sheath entrance)
L='10*DLe'; % System length(length between the wall & sheath entrance)
% numerical input parameters:
ntra=300; % Total number of trajectories at sheath entrance between vicL & vimaxL
phi0x='phi0*(1-X/L)'; % Potential at X-position iss obtained by interpolation
nx=41; % Total number of x-grids
dt=1e-11; % Time step size(s)
deltaphi=1e-7; % Desired accuracy in the iteration((phi2-phi1)>deltaphi)(volt)
w=.08; % Relaxation parameter(relating to relaxation scheme)
nv=400; % Total number of velocity grids
phifNi=linspace(-5,-0.001,1001); % Initial guess (always negative)
Tau_min=-5.8877254338; % useless to keep below: -5.8877254338, since f -> 0.
TcLiNi=linspace(-5.88,0,90); %upper limit for TpsiN=.1 -> 2.2373356648402

```

```

asymTcLiN=-4.5;          % limit below which we use the asymptotic expression

DFAMAIN

close all,                % Close all active figure, if any

clear all,                % Clear all previous data, if any

global niL vmLi vtfi kB vmaxLi vcLi Ef dx X nx    % Defining global parameters

Input                    %% input('Type the name of your input file:');

NecessaryParameters     % Gives value of constants for sheath by P-S coupling

DLe=sqrt(epsilon*kB*Tfe/neL_/e^2);    % Debye length of injected electron

L=eval(L);                % Evaluate the value of L from

vmaxLi= Tau_min*vtfi-vmLi; % Maximum injection velocity of ion at x=L

I=1;                      % Initializing the number of iteration counter

X=linspace(0,L,nx);      % Linear position grid with nx grid point between 0&L

dx=X(2)-X(1);           % x-grid mesh size

VLi=linspace(vmaxLi,vcLi,ntra); % Linear velocity grid with ntra point between
vmaxLi & vcLi

dVLi=abs(VLi(2)-VLi(1)); % Velocity mesh grid size

if dx/DLe > .8          % If Grid width is larger than Debye length ,stop the calculation

disp(' Attention: Your grid width is comparable/larger than Debye length.')

disp('Press ENTER to continue or CTRL-C to stop.')

pause

end                        % Done the calculation if grid size is less then debye length

                        % Initial guess of potential profile(given at wall & sheath entrance)

phi=eval(phi0x);phi(1)=phi0; phi(nx)=phiL;

for j=2:nx-1              % Selecting an inner jth x-grid point from 2 to nx-1.

Ef(j)=.5*(phi(j-1)-phi(j+1))/dx; % Calculate E at grid point(j) in simulation region

end                        % End of the loop started for j=2:nx-1

```



```

Ef(1)=.5*(3*phi(1)-4*phi(2)+phi(3))/dx;      % Electric field at(wall) x=0
Ef(nx)=.5*(-3*phi(nx)+4*phi(nx-1)-phi(nx-2))/dx;
DFAiondensity
ne=neL_*exp(e*phi/kB/Tfe).*(1+erf(sqrt(e*(phi-phi(1))/kB/Tfe)));
% Electron density distribution at grid point(xj)
ni=niL*ni/max(ni); ne=niL*ne/max(ne); % Check density goes off boundary region
nin=ni/niL;                                % Normalized density of ion
rho=Ze*ni-e*ne;
d=-2*ones(1,nx);                            d(1)=1;                            d(nx)=1;u=ones(1,nx-1);
% Electric field at(sheath entrance) x=L      d=-2*ones(1,nx); d(1)=1; d(nx)=1;
u=ones(1,nx-1); % Diagonal value of the Matrix of Left hand side matrix
ML=diag(d)+diag(u,1)+diag(u,-1); ML(1,2)=0;ML(nx,nx-1)=0; % Determinant of
Matrix of left hand side matrix
clear d u                                    % Clear the value of d & u
Poissonsolver
comet(X/DLe,phi)
hold, pause(.1) % Solve the poission equation and gives the new potential as 'phin'
while max(abs(phin-phi))>deltaphi % Check the fluctuation of old & new potential
I=I+1 % Next iteration
% fluctuation=max(abs(phin-phi)) % Shows the fluctuation of potential
comet(X/DLe,phi) % plot the graph between normalized distance and potential
pause(.1)
phin=phin; % Replacing the old potential by calculated new potential
for j=2:nx-1 % Selecting an inner jth x-grid point
Ef(j)=.5*(phi(j-1)-phi(j+1))/dx; % Electric field at jth point in the simulation region
end % End of loop started as for j=nx-2
Ef(1)=.5*(3*phi(1)-4*phi(2)+phi(3))/dx; % Electric field at the x=0

```

```

Ef(nx)=.5*(-3*phi(nx)+4*phi(nx-1)-phi(nx-2))/dx; % Electric field at the x=L
DFAiondensity % Calculate the new ion density using DFA
ne=neL_*exp(e*phi/kB/Tfe).*(1+erf(sqrt(e*(phi-phi(1))/kB/Tfe)));
% Electron density distribution at grid point
ni=niL*ni/max(ni); ne=niL*ne/max(ne); % Check density goes off boundary region
nin=ni/max(ni); % Normalised ion density
nen=ne/max(ne); % Normalised electron density
vcLe=sqrt(-2*e*phi0/Me); % Cut off velocity of electron at x=L
ELe=0.5*Me*vtfe^2*(0.5-vcLe*De/vtfe/Ce/sqrt(pi))/e;
Exe=0.5*Me*vtfe^2*(0.5-sqrt(e*(phi-phi(1))/kB/Tfe).*exp(-1*(e*(phi-
phi(1))/kB/Tfe))./(1+erf(sqrt(e*(phi-phi(1))/kB/Tfe)))/sqrt(pi));
Ee=Exe/e;
Een=Exe/max(Exe);
rho=Ze*ni-e*ne; % Charge density distribution for new potential profile
Poisson solver % Solving the poisson equation for new potential
end % End the calculation while max(abs(phin-phi))>deltaphi
comet(X/DLe,phi) % plot the graph between normalized distance and potential
ne=neL_*exp(e*phi/kB/Tfe).*(1+erf(sqrt(e*(phi-phi(1))/kB/Tfe)));
% Electron density distribution at grid point
ni=niL*ni/max(ni); ne=niL*ne/max(ne); % Check density goes off boundary region
nin=ni/max(ni); % Normalised ion density
nen=ne/max(ne); % Normalised electron density
ELe=0.5*Me*vtfe^2*(1.5-vcLe*De/vtfe/Ce/sqrt(pi))/e;
Exe=0.5*Me*vtfe^2*(0.5-sqrt(e*(phi-phi(1))/kB/Tfe).*exp(-1*(e*(phi-
phi(1))/kB/Tfe))./(1+erf(sqrt(e*(phi-phi(1))/kB/Tfe)))/sqrt(pi));
Ee=Exe/e;
Een=Exe/max(Exe);

```

DFAIon Density

```
Q=Ze*dt/Mi; % Defined for simplicity
for T=1:ntra % Calculate for 1-ntra
m = 1; % Initializing time counter
vxL = VLi(T); % Ion velocity for the selected trajectory at injection
Vxm = vxL; % The initial value of x-component velocity at sheath edge
Vym = -2.3045e4; % The value of y-component velocity
Vzm = -2.3045e4; % The value of z-component velocity
Vxmplus14 = Vxm +0.25*Q*DFAEfield(L)-0.25*Q*B0*Vzm*sin(Theta);
% Value of x-component velocity after at (dt/4) time
Xmplushalf = L + 0.5*dt*Vxmplus14; % Value of X moving after (dt/t) time
Vymplus14 = Vym + 0.25*Q*B0*Vzm*cos(Theta); % Value of y-component
velocity moving by (dt/4) time
Vzmpushhalf = Vzm + 0.5*Q*B0*(Vxmplus14*sin(Theta) - Vymplus14*cos(Theta))
; % Value of z-component velocity moving by (dt/4) time
Vxm(m) = Vxm; % storing the value
Vym(m) = Vym; % storing the value
Vzm(m) = Vzm; % storing the value
Xm2(m) = Xmplushalf; % storing the value
Vm2(m)= Vxm; % storing the value

if Xm2(m) <= X(nx-1) % Done only if Xm2(m) <= X(nx-1)
disp('Time step is too large. Press a key to continue.')
pause % Stop if not valid condition
end % End the loop if Xm2(m) <= X(nx-1)

while Xm2(m)>0 & Xm2(m)<=L % solving equation of motion until ion crosses
x=0 or x=L
```

```

for m=m+1                                % Next time step
Vxm(m) = Vxm(m-1) + Q*DFAEfield(Xm2(m-1))- Q*B0*Vzm(m-1)*sin(Theta);
% Value of x-component velocity moving after dt time
Vym(m) = Vym(m-1) + Q*B0*Vzm(m-1)*cos(Theta); % Value of y-component
velocity moving after dt time
Vxmminushalf = 0.5*(Vxm(m) + Vxm(m-1)); % Value of x-component velocity at
half integral centred
Vymminushalf = 0.5*(Vym(m) + Vym(m-1)); % Value of y-component velocity at
half integral centred
Vzm(m)=Vzm(m-1)+Q*B0*(Vxmminushalf*sin(Theta) - Vymminushalf*cos(Theta))
; % Value of z-component moving after dt time
Xm2(m) = Xm2(m-1) + dt*Vxm(m); % Value of position at half integral time centred
Vm2(m)=0.5*(Vxm(m)+Vxm(m-1)); % Value of x-comp. vel. at half time centred
end %Done regularly & end while Xm2(m)>0 & Xm2(m)<=L
Xt=[L,Xm2(1:m-1)]; % Position trajectory in matrix of half integral time centred
Vt=Vm2; % Corresponding velocity at half integral time centred position
a=((Xt(m-2)-Xt(m))^2*(Vt(m-1)-Vt(m-2))-(Xt(m-2)-Xt(m-1))^2*(Vt(m)-Vt(m-
2)))/(Xt(m-2)-Xt(m-1))/(Xt(m-2)-Xt(m))/(Xt(m-1)-Xt(m));
b=((Xt(m-2)-Xt(m))*(Vt(m-1)-Vt(m-2))-(Xt(m-2)-Xt(m-1))*(Vt(m)-Vt(m-
2)))/(Xt(m-2)-Xt(m-1))/(Xt(m-2)-Xt(m))/(Xt(m)-Xt(m-1));
vx0= Vt(m-2)+ a*Xt(m-2) + b*Xt(m-2)^2; % The velocoty at wall(x=0)
Xt=[Xt,0];
Vt=[Vt,vx0]; % Position (from x=L to x=0) and corresponding vel. along trajectory
Vti=interp1(Xt,Vt,X); % Interploating for the velocity at fixed grid(x)
Vi(T,:)=Vti; % Storing ion velocities at X-grid points for Tth trajectory as Tth
element of matrix VL
Df(T)=Dfun(VLi(T)); % Distribution function On (vxL=VLi(T))
clear Vm Vm2 Vt Vti Xm2 Xt a b m r vx0

```

```

end          % End of loop started as:'for T=1:ntra'

% ni calculating without interpolating onto the fixed velocity grid points

ni=zeros(1,nx);          % Initializing ni

for j=1:nx;              % Selecting j-th grid

V_xi=Vi(:,j);  % Velocities of all traced trajectories through selected j-th grid point

for T=1:ntra-1          % Integrating for ion density

ni(j)=ni(j)+.5*(Df(T)+Df(T+1))*abs(V_xi(T+1)-V_xi(T)); % Density at jth grid point

end          % End of the loop started as for j=1:ntra-1

end          % End of the loop started as for j=nx

Ei=zeros(1,nx);

Eti=zeros(1,nx);

for j=1:nx;

V_xi=Vi(:,j);

for T=1:ntra-1

j=1:nx;

Ei(j)=Ei(j)+(0.5*0.5*Mi*(V_xi(T+1).^2+V_xi(T).^2)*(Df(T)+Df(T+1))*abs(V_xi(T+1)-V_xi(T)))/(ni(j)+0.5*(Df(T)+Df(T+1))*abs(V_xi(T+1)-V_xi(T)));

Eti(j)=Ei(j)/e;

Ewi=Eti(1);

end

clear V_xi T

end

```

Coupling Scheme

% Coupling sheath with presheath.

% For given presheath plasma parameters (nps, Tpsi, Tpse, Jps, gammai, mu, etc.)
this program

% calculates sheath plasma parameters (Ai, Ae, vcLi, vmLi, Tfe, Tfi, phi0, etc.) required for our 1d3v plasma-sheath simulation.

% 1) Provide the name of your input file, where all required input parameters are specified.

% 2) Solves the electron irreducible equation to obtain 'phifN', and then the other corresponding electron parameters (TfeN, AeN, phi0N, etc.) are calculated.

% 3) Solves the ion irreducible equation to obtain 'TaucLiN', and then the other corresponding ion parameters (TfiN, AiN, vmLiN, vcLiN, etc.) are calculated.

% 4) Once all normalized parameters are known, the dimensionless physical parameters are calculated

% using their respective normalizing equations solving the electron irreducible equation for 'phifN' --- start --- :

% Calculating the lhs (Le) of the equation (independent of 'JpsN' & 'TpsiN'):

for rphifN=1:length(phifNi)

phifN=phifNi(rphifN);

Ce=1+erf(sqrt(-phifN));

De=exp(phifN);

TfeN=1/abs(1 - sqrt(-4*phifN/pi)*De/Ce - 2/pi*(De/Ce)^2);

Le(rphifN)=De/Ce*sqrt(TfeN/pi); % lhs of the electron irreducible equation

end %for r=1:length(phifNi)

% Calculating the rhs (Re) of the equation (function of 'JpsN', 'TpsiN', 'gammai' and 'mu'):

Re=sqrt(mu)*(JpsN+sqrt(.5*(1+gammai*TpsiN))); % rhs of the equation

phifN_sol=interp1(Le, phifNi, Re); % Interpolating for the solution (phifN) for which Le = Re.

% Thus obtained 'phifN_sol' is the required value.

if isnan(phifN_sol)

disp('Could not find the solution. Change the input-range for phifN and start again.')

```

pause

else

phifN=phifN_sol          % Calculating other parameters:

Ce=1+erf(sqrt(-phifN));

De=exp(phifN);

TfeN=1/abs(1 - sqrt(-4*phifN/pi)*De/Ce - 2/pi*(De/Ce)^2);

AeN=1/Ce/sqrt(TfeN);

end % if isnan(phifN_sol)

% solving the electron irreducible equation for 'phifN' --- end ---

% solving the ion irreducible equation for 'TcLiN' ----- start -----

% Calculating the rhs (Ri) of the equation (function of 'phifN'; independent of 'JpsN'
& 'TpsiN'):

Ri=(sqrt(pi) + De/Ce/sqrt(-phifN))/TfeN;

% Calculating the lhs (Li) of the equation:

rr=1;

for r=1:length(TcLiNi)

TcLiN=TcLiNi(r);

if TcLiN<asymTcLiN

% using asymptotic expansion: erf(x)=1-exp(-x^2)/sqrt(pi)/x*(1 - 1/2/x^2 + 3/2^2/x^4
- 1.3.5/2^3/x^6 + ...)

Ci=exp(-TcLiN^2)/abs(TcLiN)/sqrt(pi)*(1 - .5/TcLiN^2 + .75/TcLiN^4 -
15/8/TcLiN^6 + 105/16/TcLiN^8 - ...

945/32/TcLiN^10 + 10395/64/TcLiN^12 - 135135/128/TcLiN^14 +
2027025/256/TcLiN^16 - 34459425/512/TcLiN^18 + ...

654729075/1024/TcLiN^20 - 13749310575/2048/TcLiN^22 +
316234143225/4096/TcLiN^24 - 7905853580625/8192/TcLiN^26);

else %if TcLiN<asymTcLiN

```

```

Ci=1+erf(TcLiN);
end %if TcLiN<asymTcLiN

Di=exp(-TcLiN^2);

TfiN=TpsiN/abs(1 - 2*TcLiN*Di/Ci/sqrt(pi) - 2*(Di/Ci)^2/pi);
vmLiN=-sqrt(0.5*(1+gammai*TpsiN)) + Di/Ci*sqrt(TfiN/pi);
a=vmLiN/sqrt(TfiN); % abbreviated for simplicity

if TcLiN < -a % checking the integerability

Tau=linspace(Tau_min,TcLiN,ntra); % Discretizing for integration
dTau=Tau(2) - Tau(1); % Width of the Tau-grid

for rTau=1:ntra

FnTau(rTau)=exp(-Tau(rTau)^2) / (Tau(rTau) + a)^2;

end

LHS = dTau * ( sum(FnTau) - 0.5*(FnTau(1) +FnTau(ntra)) );

Li(rr) = LHS/Ci/TfiN;

TcLiNM(rr)=TcLiN; % storing the values for which the equation is integrable.

rr=rr+1;

end % if TcLiN < -a

end %for r=1:length(phifNi)

% obtaining the solution by locating the point of intersection of 'Li' & 'Ri':

%%plot(TcLiNM, Li)

%%hold

%%plot([min(TcLiNM) max(TcLiNM)],[Ri Ri],'k--')

TcLiN_sol=interp1(Li,TcLiNM,Ri); % required solution

% This method of obtaining the solution can be RISKY. The point where we have
found 'Li=Ri' is

% the point of marginal validity of the Bohm's criterion, which, in our case, is Li <=
Ri. When we consider the marginal point it may be possible that because of numerical

```


limitations it lies in fact in the region, where the Bohm's criterion is not satisfied. Hence, in order to be sure we take a point very close to the zero-point but still lying in the negative side of sure side of $(Li - Ri)$, so that we may say that $Li \ll Ri$, in place of $Li \leq Ri$.

% We have tested it many times and concluded that it has also negligible effect to the other ion parameters derived there from.

```

a=find(Li-Ri<0);           % points where Li < Ri
a=a(length(a));           % points closest to the zero-point but still Li < Ri
TcLiN_sol=TcLiNM(a);      % value of the closest point to the zero-point => Li << Ri
%plot(TcLiNM(a), Li(a),'mo')
% solving the ion irreducible equation for 'TcLiN' ----- end -----
% calculating other dimensionless ion parameters:
% Thus obtained 'TcLiN_sol' is the required value.
if isnan(TcLiN_sol)
disp('Could not find the solution. Change the input-range for TcLiN and start again.')
pause
else
TcLiN=TcLiN_sol           % Calculating other parameters:
if TcLiN<asymTcLiN
% using asymptotic expansion: erf(x)=1-exp(-x^2)/sqrt(pi)/x*(1 - 1/2/x^2 + 3/2^2/x^4
- 1.3.5/2^3/x^6 + ...)
Ci=exp(-TcLiN^2)/abs(TcLiN)/sqrt(pi)*(1 - .5/TcLiN^2 + .75/TcLiN^4 -
15/8/TcLiN^6 + 105/16/TcLiN^8 - ...
945/32/TcLiN^10 + 10395/64/TcLiN^12 - 135135/128/TcLiN^14 +
2027025/256/TcLiN^16 - 34459425/512/TcLiN^18 + ...
654729075/1024/TcLiN^20 - 13749310575/2048/TcLiN^22 +
316234143225/4096/TcLiN^24 - 7905853580625/8192/TcLiN^26);
else
%if TcLiN<asymTcLiN

```

```

Ci=1+erf(TcLiN);
end    %if TcLiN<asymTcLiN

Di=exp(-TcLiN^2);

TfiN=TpsiN/abs(1 - 2*TcLiN*Di/Ci/sqrt(pi) - 2*(Di/Ci)^2/pi);

vmLiN=-sqrt(0.5*(1+gammai*TpsiN)) + Di/Ci*sqrt(TfiN/pi);

AiN=1/Ci/sqrt(TfiN);

vcLiN=vmLiN + TcLiN*sqrt(TfiN);

end          %if isnan(TcLiN_sol)

% calculating dimensional physical parameters:

% electron dimensional parameters:

Tfe=TfeN*Tpse;

vtfe=sqrt(2*kB*Tfe/Me);

Ae=AeN*nps*sqrt(2*Me/pi/kB/Tpse);

neL_=Ae*vtfe*sqrt(pi)/2;

phi0=phifN*kB*Tfe/e;

% ion dimensional parameters:

Tfi=TfiN*Tpse;

vtfi=sqrt(2*kB*Tfi/Mi);

Ai=AiN*nps*sqrt(2*Mi/pi/kB/Tpse);

niL=nps;

vmLi=vmLiN*sqrt(2*kB*Tpse/Mi);

vcLi=vcLiN*sqrt(2*kB*Tpse/Mi);

Particle Absorption

% Reflecion coefficient of carbon at wall clc

Viw=Vi(:,1)';          % Velocity of ion at wall

Energywall=0.5*Mi*(Viw).^2/(1.6e-19);          %energy at wall

```

```

Energy_reflection=find(10<Energywall<100000);
EF=Energywall(Energy_reflection); %element with energy more than threshold
EOC=sum(Energywall(Energy_reflection));
Lm=length(Energy_reflection);
Vmth=Viw(Energy_reflection); %velocity of ion corresponding to Emth
%Check the density goes out of the boundary region.
Thomas_Fermi_energy_carbon=32.5*(m2c/(m1+m2c))*1/(z1*z2c*(z1^(2/3)+z2c^(2/3))^(1/2)); %Thomas Fermi energy for carbon
Ac1=0.6192; Ac2=20.01; Ac3=8.922; Ac4=0.6669; Ac5=1.864; Ac6=1.899;
RFE=EOC*Thomas_Fermi_energy_carbon; %Thomas_fermi_reduced_energy
RC=Ac1*log(Ac2*RFE+2.718)/(1+Ac3*RFE^Ac4+Ac5*RFE^Ac6);
niC=(1-RC)*ni(1); %ion density at wall
niRC=RC*ni(1); %reflected ion density from wall
rhoC=e*(niC-ne(1)); %total charge density
% Reflection coefficient of tungsten wall
Thomas_Fermi_energy_tungsten=32.5*(m2w/(m1+m2w))*1/(z1*z2w*(z1^(2/3)+z2w^(2/3))^(1/2)); %Thomas Fermi energy for carbon
Aw1=0.8250; Aw2=21.41; Aw3=8.606; Aw4=0.6425; Aw5=1.907; Aw6=1.927;
RFEW=EOC*Thomas_Fermi_energy_tungsten; %Thomas_fermi_reduced_energy
RW=Aw1*log(Aw2*RFEW+2.718)/(1+Aw3*RFEW^Aw4+Aw5*RFEW^Aw6);
niW=(1-RW)*ni(1); %ion density at wall
niRW=RW*ni(1); %reflected ion density from wall
rhoW=e*(niW-ne(1));

```